AN INVESTIGATION INTO THE EFFICIENCY AND EMBODIED ENERGY OF ELECTRIC MOTORS FOR USE IN PUMPING

Clinton Smythe

A research report submitted to the Faculty of Engineering and the Built Environment, University of the Witwatersrand, Johannesburg, in partial fulfilment of the requirements for the degree of Master of Science in Engineering.

Johannesburg, 2011

Declaration

I declare that this research report is my own, unaided work, other than where specifically acknowledged. It is being submitted for the degree of Master of Science in Engineering in the University of the Witwatersrand, Johannesburg. It has not been submitted before for any degree or examination in any other university.

Signed this _____ day of _______________ 2011

____

Clinton Smythe

Abstract

This research report is separated into two sections. The first section covers the embodied energy which is required to manufacture a new electric motor. It takes into account the energy required to mine, transport and process all raw materials, as well as the energy used by the factory to turn the raw materials into a motor. The second section investigates the actual efficiency of a pumping system under various operating conditions, these include changing the static head, changing the throttling of a valve, and changing the supply frequency. Two 0.37 kW induction motors are used, an energy efficient motor and a standard motor. The differences in efficiency between two motors is compared under each of the different test conditions. The analysis is also taken a step further as the efficiency of each of the subsystems is investigated in isolation, rather than simply looking at the overall efficiency of the system. This provided valuable information about how the system could be made more efficient, as well as an understanding as to where the losses in the system occur.

Finally the two sections are combined so that one is able to decide whether it is worth upgrading to a new more efficient motor or stick with the existing motor. Although there may be efficiency improvements by using the new motor, there is also an upfront embodied energy which was required to manufacture the motor. The two pieces of information will give a payback period, if the motor is operated less than the payback period then more energy is in fact used to manufacture the motor than the motor actually saves due to improved efficiency.

This work is dedicated to my parents for providing endless opportunities for success.

Acknowledgements

This research was performed under the auspices of the Machines Research Group at the University of the Witwatersrand. Firstly I would like to thank my supervisor Prof. Willie Cronje for his support and guidance for the duration of the project. I would also like to extend thanks to the rest of the research group for their feedback at our weekly meetings, and in particular Mr. Alan Meyer for sharing his knowledge of machines in industry.

Special mention should go to all the staff in the Genmin Laboratory Workshop for their assistance in any tooling that was required for the project. In particular I would like to thank Mr. Harry Fellows.

It is important to note that none of this would have been possible without my parents. I appreciate the interest they showed in my research and their motivation for me to finish when procrastination seemed like the path of least resistance.

Contents

List of Figures

List of Tables

Chapter 1

Introduction

In industry the use of electric motors is widespread for numerous applications. Pumping is the single largest application of motive power with fans also contributing significantly to the total energy consumption. The three phase induction motor is the most widely used motor in industry [1]. Global warming and other environmental concerns, as well as the rapidly increasing price of electricity in South Africa have contributed to the drive to save energy. Table 1.1 shows the past and future prices of electricity in South Africa.

Table 1.1: Past and Future Electricity Prices [2]

Period			**Price**	**Increase on Previous**	**Increase on 30 June 2009**
		30 June 2009	25.24 c/kWh		
1 July 2009	–	31 March 2010	33.14 c/kWh	31.3%	31.3%
1 April 2010	–	31 March 2011	41.31 c/kWh	24.8%	63.7%
1 April 2011	–	31 March 2012	51.68 c/kWh	25.8%	104.8%
1 April 2012			65.06 c/kWh	25.9%	157.8%

The efficient use of electricity has become a national priority, and a necessity for the future development of the South African economy. Eskom's Accelerated Energy Efficient Plan therefore has set targets to reduce the national demand by 3 000 MW by 2012 and a further 5 000 MW by 2025 [3]. Industry is a major consumer of electricity where an estimated 100 000 motors consume up to 10 GW of electrical power. This accounts for about 60% of all electrical power used by industry. Clearly improving the efficiency of these motors could play a pivotal role in meeting Eskom's energy targets. Thus Eskom has introduced the Energy Efficient Motors (EEM) programme, which offers users subsidies when trading in old motors for new energy efficient motors. The old motors are then scrapped to ensure that those *inefficient* motors cannot be reused [4]. Superficially this Eskom Demand Side Management (DSM) policy may seem quite reasonable, however this research aims to investigate the deeper implications of such a policy. The efficiency classes and rebates offered by the EEM programme are given in table 1.2.

Table 1.2: Subsidies Offered by the EEM Programme [4, 5]

kW	**Eff1**		**Eff2**	**DSM**
Rating	**2–Pole**	**4–Pole**	**(All)**	**Subsidy**
1.1	82.8%	83.8%	76.2%	R 400
1.5	84.1%	85.0%	78.5%	R 400
2.2	85.6%	86.4%	81.0%	R 500
3	86.7%	87.4%	82.6%	R 500
4	87.6%	88.3%	84.2%	R 500
5.5	88.6%	89.2%	85.7%	R 700
7.5	89.5%	90.1%	87.0%	R 700
11	90.5%	91.0%	88.4%	R 700
15	91.3%	91.8%	89.4%	R 700
18.5	91.8%	92.2%	90.0%	R 1 000
22	92.2%	92.6%	90.5%	R 1 300
30	92.9%	93.2%	91.4%	R 1 400
37	93.3%	93.6%	92.0%	R 1 700
45	93.7%	93.9%	92.5%	R 2 200
55	94.0%	94.2%	93.0%	R 2 600
75	94.6%	94.7%	93.6%	R 3 000
90	95.0%	95.0%	93.9%	R 3 500

1.1 Research Objectives

The research follows two seemingly independent paths: *(i)* the embodied energy required to manufacture a new motor; and *(ii)* the efficiency of a pumping system under different operating conditions. These paths however meet again when we try estimate the energy payback period when replacing an standard motor with an energy efficient motor.

The structure of this research report is as follows:

Chapter 2: Embodied Energy Estimate
In this chapter, with the assistance of Actom (formerly Alstom South Africa), we

estimate the embodied energy of the various different electrical induction motors. The motors range from 200 kW to 6 500 kW. In order to make decisions about energy saving, it is necessary to know how much energy is spent upfront to manufacture a new motor.

Chapter 3: Pumping Efficiency Tests

In this chapter, the pumping tests are discussed. The testing involved comparing the system efficiency while changing the static head, the supply frequency and the position of a ball valve. Each test is also performed with both a standard and an energy efficient 0.37 kW induction motor. A list of system components and a description of the test setup it given before delving into the actual test results. The testing aimed to find the efficiency of the various subsystems of the pumping setup, and compare the effects of the various changes. This will help to optimise the efficiency of each subsystem, and give a better understanding of where the main losses are in the system.

Chapter 4: Energy Payback Period

This chapter combines the embodied energy of chapter 2 and the efficiency comparison between the standard and energy efficient motors of chapter 3. Unfortunately since the embodied energy study was performed on motors ranging from 200 kW to 6 500 kW, and the pumping tests used 0.37 kW motors, it is difficult make definitive conclusions in the study. Extrapolation of the embodied energy data becomes necessary, and immediately adds a source of errors. However despite these problems, the payback periods of the motors was estimated. One is now able to make calculated decisions about replacing the motor. The decision of whether replacing the motor will save energy or not, can now be made by finding the embodied energy of the motor and the expected efficiency differences.

Appendix A: The Rig for Measuring Torque

The running torque at the output of the motor and input to the pump is necessary to calculate the rotational mechanical energy during the test. The design considerations for measuring the torque are given in this appendix. While the torque measurement rig works in theory, it proved to be too inaccurate in practice. The main problem with the system was friction.

Appendix B: Torque Estimate by Modelling the Motors

This appendix showed that by modelling the motors themselves, the output power and torque of the motors could be determined. The motors were modelled using the induction motor per phase equivalent circuit. Locked rotor and no load tests were performed at various frequencies, and a genetic algorithm solver was used to optimise the equivalent circuit parameters. By performing no load tests both with and without the gearbox, the friction and windage losses of the motor and the gearbox could be estimated separately.

Appendix C: Torque Estimate by Modelling the Pump

The torque is estimated by modelling the pump in this appendix. Since the output pressure and flow rate and the angular velocity of the pump were measured, the input power and therefore torque can be read off a data sheet. The data sheet curves however only show the characteristics at a few discrete frequencies, and the challenge was in interpolating the resulting surface find the characteristics at other frequencies.

Appendix D: Tabulated Pumping Test Results

This appendix gives the averages of the values measured during the 96 tests performed. Instead of having one large table, the readings have been split into a number of smaller tables. Each table describes the measurements of a different subsystem.

Chapter 2

Embodied Energy Estimate

The term embodied energy is the total energy necessary to manufacture and maintain a product for its entire life cycle. The embodied energy of an electric motor is therefore the total energy which goes into manufacturing and maintaining the motor [6–8].

Embodied energy can be divided into two categories:

- The initial embodied energy represents the non-renewable energy consumed in the acquisition of raw materials, their processing, transportation and finally the manufacture of the motor itself.
- The recurring embodied energy represents the non-renewable energy consumed to maintain, repair, restore, refurbish or replace components during the remaining life of the motor.

In this chapter, we will only consider the initial embodied energy.

2.1 Approach and Assumptions

With the assistance of Actom (formerly Alstom South Africa), the embodied energy of various induction motors ranging from 200 kW to 6 500 kW were estimated. The data covered a one year period.

The mass of all copper and steel purchases over that period were tallied. Although other materials form part of the motor, steel and copper are by far the largest contributors so all others have been neglected. Various sources estimate the embodied energy in copper and steel [6–12], and these values were used for the estimate. Additionally the utility bills for the plant have also been made available, and the monthly energy costs (electricity and gas) were included in the analysis.

By adding the raw materials component of embodied energy (steel and copper) to the energy used by the factory (electricity and gas) over the period, we could estimate the total embodied energy for all motors produced during the period. Finally this total embodied energy needed is to be divided appropriately between all motors manufactured during that period so that the embodied energy for a single motor could be obtained.

Since the steel and copper are large contributors to the embodied energy of each motor, it is reasonable to assume that the raw materials component of the embodied energy of each motor is proportional to its mass. Also since the electricity and gas can only contribute to the embodied energy while the motor is actually being manufactured, we assumed that the gas and electricity portion of the embodied energy was proportional to the lead time for that motor.

Finally since the lead time of some of the larger motors can be up to nine months, it is likely that some of the motors which are considered to be manufactured during the period were started many months earlier. Also many of the motors started during the period will not be finished and therefore not counted. However, since the factory output over the period and for a few months before were fairly constant, we shall assume that the two effects cancel out.

2.2 The Motor Data

Table 2.1 shows the motors which were manufactured over the considered one year period. The motor power ratings were divided into four classes, where each class includes a different range of motor ratings. The motors were also divided into squirrel cage and wound rotor induction motors. Since class A and B do not include wound rotor motors, a total of six groups were considered.

Table 2.1: Actom Motor Data for the Period

Motor Class	kW Rating Range		Total kW Ratings			Number Manufactured			Average kW Rating		
	Min	Max	Cage	Wound	Total	Cage	Wound	Total	Cage	Wound	Total
A	200	720	46 827	-	46 827	138	-	138	339.33	-	339.33
B	660	1700	34 060	-	34 060	30	-	30	1 135.33	-	1 135.33
C	683	2700	80 306	37 238	117 544	46	20	66	1 745.78	1 861.90	1 780.97
D	2985	6500	13 200	64 803	78 003	4	15	19	3 300.00	4 320.20	4 105.42
Total	-	-	174 393	102 041	276 434	218	35	253	799.97	2 915.46	1 092.62

2.3 Method for Generating a List of Motors

In order to continue the analysis, we would ideally like to have a complete list of motors manufactured over the period including their power rating, mass and manufacturing lead time. However since only a summary of the motors manufactured during the period was made available, the next step was to generate a list of motors which would be most representative of the data given in table 2.1.

The list of motors was generated by assigning a Probability Density Function (PDF) and its associated Cumulative Density Function (CDF) for each group of motors [13]. PDFs and CDFs are most commonly used in statistics to describe probabilities, in this instance however we are simply using them as a tool to generate a list of motors to fit the data in table 2.1. It is a deterministic algorithm, and has nothing at all to do with probability.

The PDFs were developed as follows:

1. Define a temporary function over the range from X_{start} to X_{end} (this function should be strictly non-negative). It is used to describe the shape of the PDF.

$$g(x) = t(x) \tag{2.1}$$

2. Find the area under the curve of equation 2.1.

$$G(x) = \int_{X_{start}}^{x} g(\chi)\ d\chi \tag{2.2}$$

3. Convert equation 2.1 into a PDF by ensuring that the area under the curve equals one.

$$f(x) = \frac{g(x)}{G(X_{end})} \tag{2.3}$$

4. Convert equation 2.2 into a CDF by ensuring the the final cumulative probability equals one.

$$F(x) = \frac{G(x)}{G(X_{end})} \tag{2.4}$$

Once we have generated the PDF and CDF we are able to generate the list of motors. This is illustrated in figure 2.1. This example shows a list of motors generated for the class D wound rotor motors (2 985 kW to 6 500 kW). Each of the vertical lines from the PDF and CDF represents a motor. Since the CDF will be steeper at the points of higher probability, by evenly spacing horizontal lines on the y–axis the

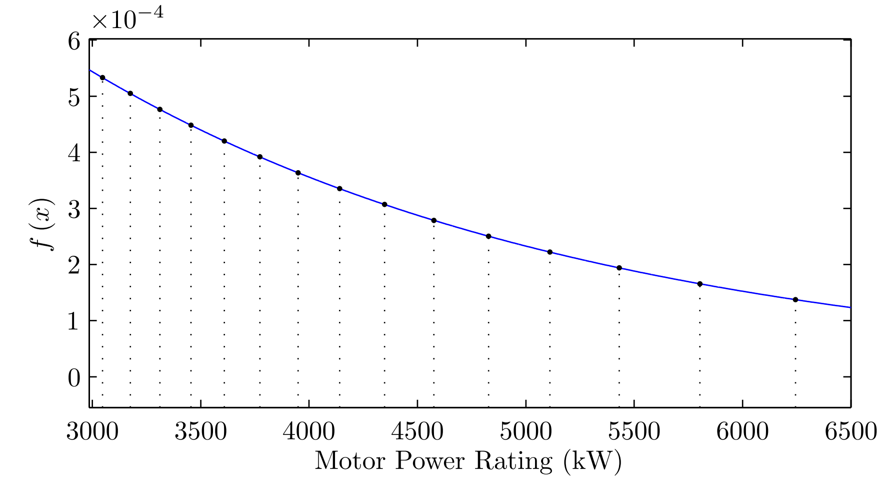

(a) The Probability Density Function

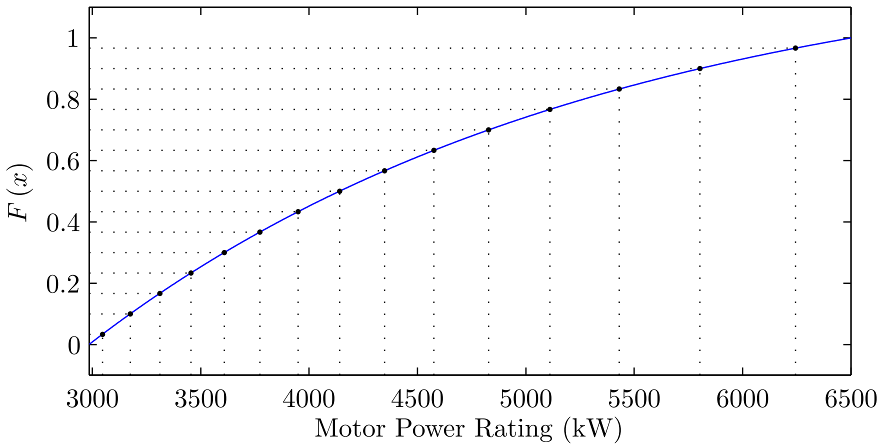

(b) The Cumulative Density Function

Figure 2.1: An Example using a PDF and CDF to Generate a List of Motors

corresponding x–values will be the list of motor power ratings. The 15 vertical lines represent the 15 motors in this group, and it is clear that the density of motors is higher at higher probabilities. In this example there are more motors near the lower power ratings so that the correct average for the group is obtained.

This method should be applied to each of the six groups of motors from table 2.1. Combining the results will then create a complete list of all motors manufactured over the period.

2.4 A Description of the Distributions

The following four functions were used in the analysis. The horizontal asymptotes ensure that all of the chosen functions are strictly non-negative. Four different functions were chosen to compare the effect of using different distributions. These functions should be converted to a PDF and CDF using steps described in equations 2.1 to 2.4.

$$g_0(x) = 1 \tag{2.5}$$

$$g_1(x) = \delta(x - X_{av}) \tag{2.6}$$

$$g_2(x) = e^{k\frac{x - X_{av}}{X_{range}}} \tag{2.7}$$

$$g_3(x) = 1 + \tanh\left(k\,\frac{x - X_{av}}{X_{range}}\right) \tag{2.8}$$

where

$g_n(x)$ = Temporary function which describes the shape of the PDF (non-normalised PDF)

k = The slope constant for the distribution

X_{start} = The minimum power rating for the range of motors (kW)

X_{end} = The maximum power rating for the range of motors (kW)

X_{av} = The average power rating for the range of motors (kW)

X_{range} = The difference between maximum and minimum power Rating (kW)

2.4.1 The Uniform Distribution

Without any prior knowledge of the average power rating of a set of motors, a reasonable approach would be to evenly distribute the motors over the entire range. Equation 2.5 would achieve this result. For the case of the Actom data provided in in table 2.1, this will not be an accurate representation since the average power rating for each group of motors has been given and should be taken into account. For that reason the uniform distribution is not recommended.

The PDF and CDF for equation 2.5 are as follows (an example is shown in figure 2.2):

$$f(x) = \frac{1}{X_{range}} \tag{2.9}$$

$$F(x) = \frac{x - X_{start}}{X_{range}} \tag{2.10}$$

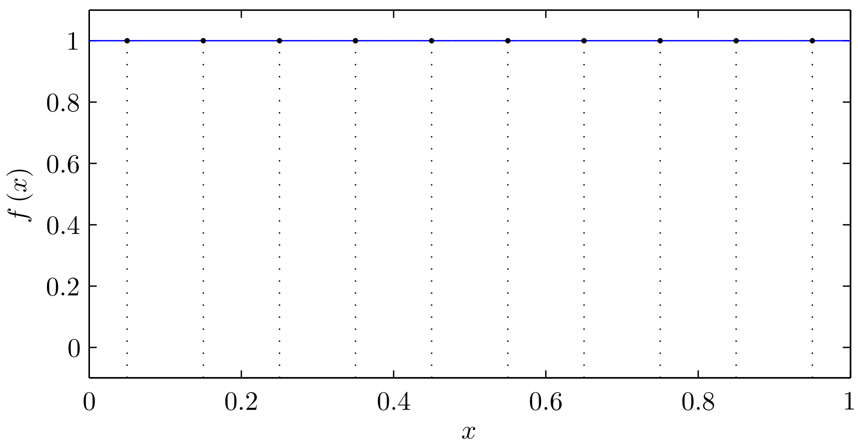

(a) The Probability Density Function

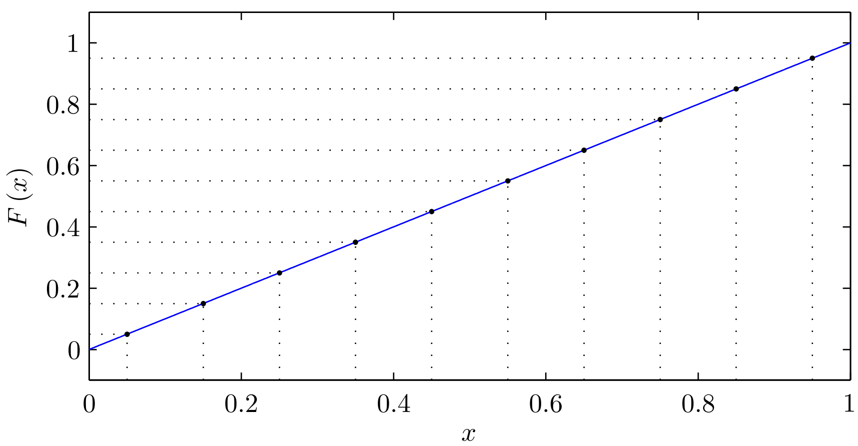

(b) The Cumulative Density Function

Figure 2.2: An Example of the Uniform Distribution

2.4.2 The Impulse Distribution

Another simple distribution would be to simply clump all of the manufactured motors at the average power rating for each group. This will take into account the average power rating of the data, and should therefore model the data more accurately. This is achieved by the distribution from equation 2.6. A criticism of this approach is that it is implicit that there is a spread of motors power ratings since each group specifies a range of values (rather than just a single value).

The PDF and CDF for equation 2.6 are as follows (an example is shown in figure 2.3):

$$f(x) = \delta(x - X_{av}) \tag{2.11}$$

$$F(x) = \mathrm{u}(x - X_{av}) \tag{2.12}$$

where

$\delta(x)$ = The Dirac Delta Function

$\mathrm{u}(x)$ = The Heaviside Step Function

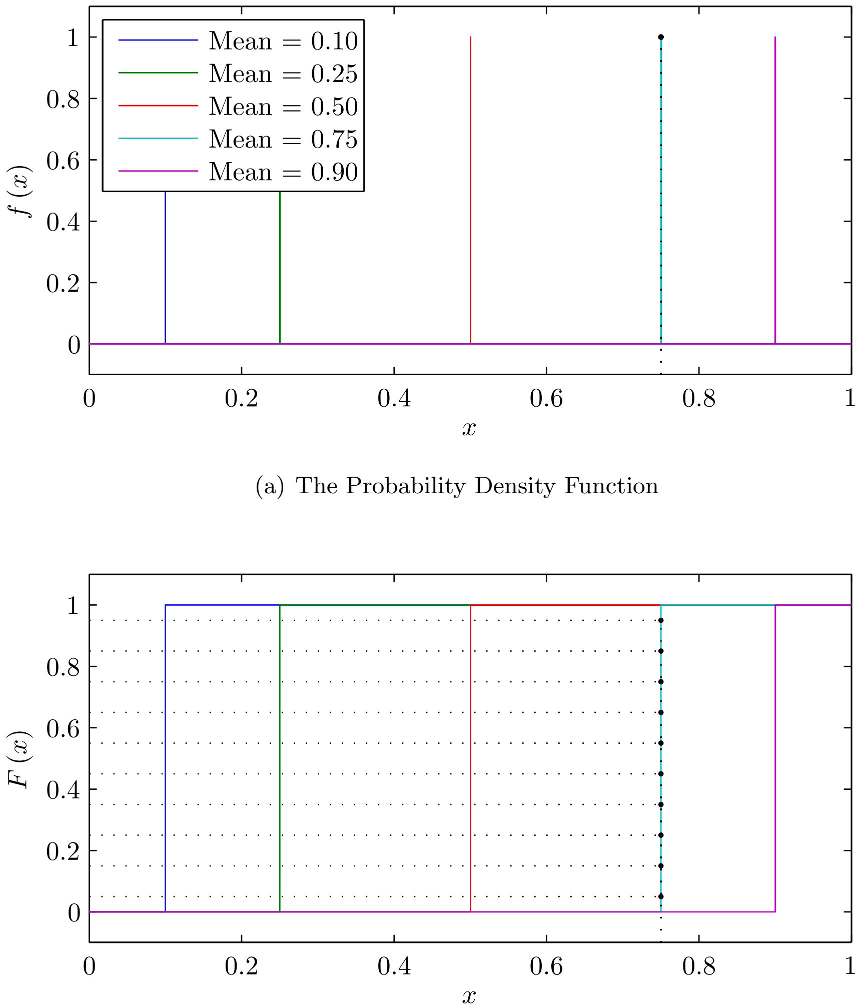

(a) The Probability Density Function

(b) The Cumulative Density Function

Figure 2.3: An Example of the Impulse Distribution

2.4.3 The Exponential Distribution

The exponential distribution is more complicated than the previous two distributions, however it is able to generate a range of motors which have the correct average.

Equation 2.7 distributes the list of motors according to an exponential function. This function will both distribute the list of motors over the whole range of motor power ratings, but will also be able to correctly take into account the average power rating. The slope coefficient k should be adjusted so that the list of motors generated has the correct average as specified in table 2.1. Essentially k is a function of X_{start}, X_{end}, X_{av} and the number of motors in the range, but is much too complicated to solve analytically. A variation on the Newton–Rhapson method was used to find k.

The PDF and CDF for equation 2.7 are as follows (an example is shown in figure 2.4):

$$f(x) = \frac{\frac{k}{X_{range}}\, e^{k\,\frac{x - X_{av}}{X_{range}}}}{e^{k\,\frac{X_{end} - X_{av}}{X_{range}}} - e^{k\,\frac{X_{start} - X_{av}}{X_{range}}}} \tag{2.13}$$

$$F(x) = \frac{e^{k\,\frac{x - X_{av}}{X_{range}}} - e^{k\,\frac{X_{start} - X_{av}}{X_{range}}}}{e^{k\,\frac{X_{end} - X_{av}}{X_{range}}} - e^{k\,\frac{X_{start} - X_{av}}{X_{range}}}} \tag{2.14}$$

2.4.4 The Hyperbolic Tangent Distribution

Finally equation 2.8 distributes the list of motors according to a hyperbolic tangent function. Since this function has an upper (as well as a lower) asymptote, the list of generated motors will not bunch as much at one of the edges of the range, but should be distributed slightly more evenly. This comes at the expense of additional complexity. As before the constant k is solved using a variation on the Newton–Rhapson method.

The PDF and CDF for equation 2.8 are as follows (an example is shown in figure 2.5):

$$f(x) = \frac{k\,\left(1 + \tanh\left(k\,\frac{x - X_{av}}{X_{range}}\right)\right)}{k\,\left(X_{end} - X_{start}\right) + X_{range}\,\ln\left(\frac{\cosh\left(k\,\frac{X_{end} - X_{av}}{X_{range}}\right)}{\cosh\left(k\,\frac{X_{av} - X_{start}}{X_{range}}\right)}\right)} \tag{2.15}$$

$$F(x) = \frac{k\,\left(x - X_{start}\right) + X_{range}\,\ln\left(\frac{\cosh\left(k\,\frac{x - X_{av}}{X_{range}}\right)}{\cosh\left(k\,\frac{X_{av} - X_{start}}{X_{range}}\right)}\right)}{k\,\left(X_{end} - X_{start}\right) + X_{range}\,\ln\left(\frac{\cosh\left(k\,\frac{X_{end} - X_{av}}{X_{range}}\right)}{\cosh\left(k\,\frac{X_{av} - X_{start}}{X_{range}}\right)}\right)} \tag{2.16}$$

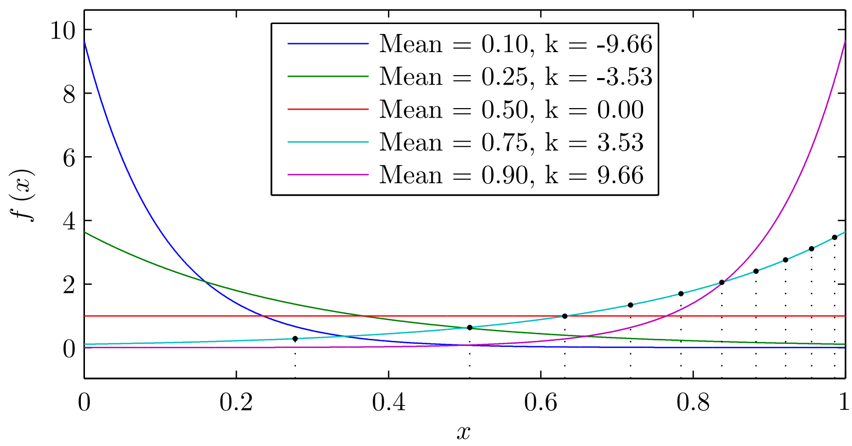

(a) The Probability Density Function

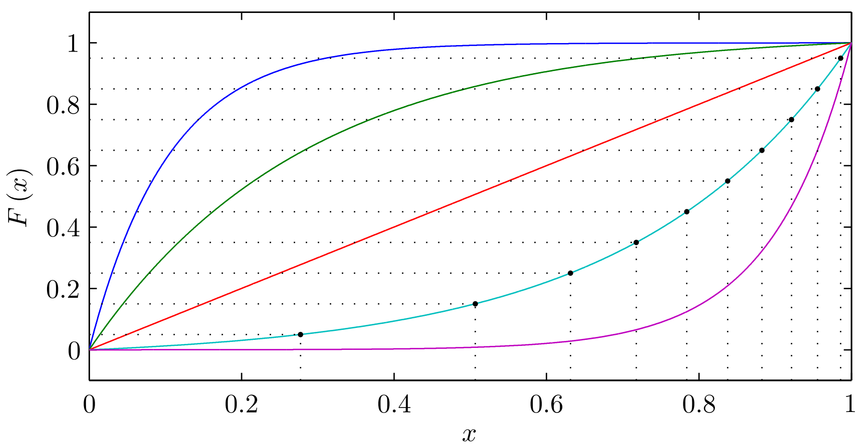

(b) The Cumulative Density Function

Figure 2.4: An Example of the Exponential Distribution

Table 2.2: Slope Coefficients for the Exponential and Hyperbolic Tangent Distributions

Motor Group	**Slope Coefficient** (k) **Exponential**	**Hyperbolic Tangent**
A – Cage	-3.2387	-2.6513
B – Cage	-0.5174	-0.5108
C – Cage	0.3234	0.3218
C – Wound	1.0301	0.9847
D – Cage	-10.2199	-7.7554
D – Wound	-1.4901	-1.3727

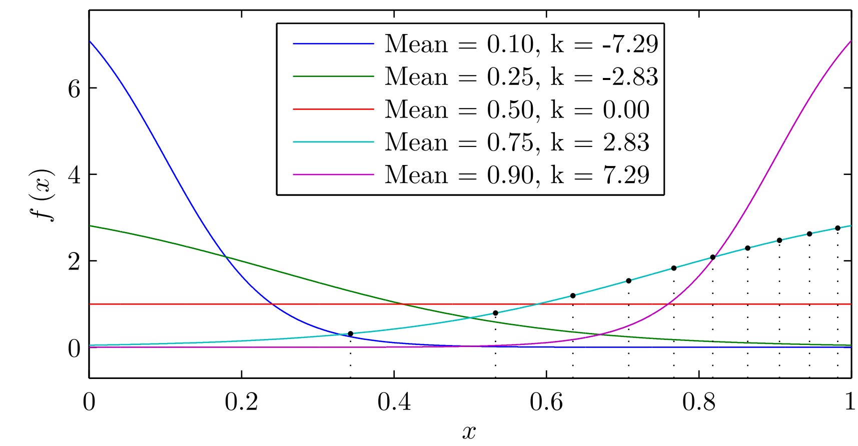

(a) The Probability Density Function

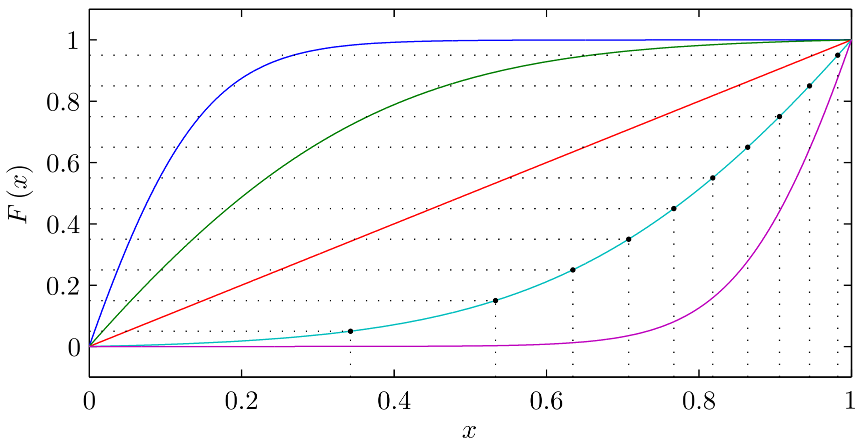

(b) The Cumulative Density Function

Figure 2.5: An Example of the Hyperbolic Tangent Distribution

2.5 Total Embodied Energy

Once the list of motors has been generated, each motor in the list was assigned an embodied energy. The total embodied energy of all the motors in the list must correspond to raw materials, gas and electricity used during the period.

2.5.1 Raw Materials Component

According to the data from Actom about 3 248 000 kg of steel and 215 000 kg of Copper were used over the period. The exact embodied energy depends on the grade of steel used for the motors, and also whether virgin steel and copper is used or if it is recycled. Due to their weight, steel and copper are high in embodied energy when it comes to transporting it over large distances. Additionally different mining techniques are used at different locations, therefore it is difficult to get an exact value for the embodied energy of the raw materials of the motors. The embodied energy of steel was estimated to be 32.0 MJ/kg (8.89 kWh/kg), and 70.6 MJ/kg (19.6 kWh/kg) was used for copper [6, 8–10, 12].

Table 2.3: Embodied Energy of Raw Materials

		Embodied Energy		
	mass	**Per Unit**	**Total**	
	kg	MJ/kg	MJ	kWh
Steel	3 248 000	32.0	103 936 000	28 871 111
Copper	215 000	70.6	15 179 000	4 216 389
Total	3 463 000	-	119 115 000	33 087 500

2.5.2 Electricity and Gas Component

The manufacturer also used about 3 863 200 units of electricity and 193 314 units of gas over the one year period. Each unit of electricity corresponds to 3.6 MJ (1 kWh). Each unit refers to 1 m^3 (at STP) and has an energy content of 40.393 MJ/m^3 (11.220 kWh/m^3).

Table 2.4: Embodied Energy of Electricity and Gas

		Energy Content		
	Units	**Per Unit**	**Total**	
		MJ/unit	MJ	kWh
Electricity (kWh)	3 863 200	3.6	13 907 520	3 863 200
Gas (m^3)	193 314	40.393	7 808 532	2 169 037
Total	-	-	21 716 052	6 032 237

Therefore the total embodied energy (raw materials, electricity and gas) of all motors manufactured during the period was 140 831 052 MJ (39 119 737 kWh).

2.6 Embodied Energy of Each Motor

2.6.1 Mass and Lead Time of the Motors

As discussed earlier we assumed that the raw materials component of the embodied energy is proportional to the mass of the motor. The electricity and gas component of the embodied energy was assumed to be proportional to the lead time for the motor. The relationship for the mass and lead time of a motor as a function of its power rating must therefore be determined.

Actom supplied the data in table 2.5 which shows the mass and lead times of motors of different power ratings.

Table 2.5: Mass and Lead Time Data

Power Rating kW	**Mass** kg	**Lead Time** weeks	**Weighting Factor**	
425	3 350	10	(A)	138
995	4 250	10	(B&C)	10+11
1 000	5 680	10	(B&C)	10+11
1 500	8 100	15	(B&C)	10+11
1 800	9 680	15	(C)	11
2 000	12 100	15	(C)	11
2 240	16 060	18	(C)	11
2 985	22 380	21	(D)	6.3
3 300	29 680	23	(D)	6.3
4 476	32 300	25	(D)	6.3

A second order polynomial is used to fit the mass and lead time data. Figure 2.6 shows second order polynomial least squares fit for both the mass and lead time. Each figure includes two fits, one where each of the data points have been weighted and the other without weighting.

In the mass fit without weights, the mass goes negative for the small motors (around 200 kW). Clearly this cannot be correct. The problem is exaggerated since the majority (about 35%) of the motors have power ratings less than 350 kW which is where the curve starts going negative. If anything the fit should be most accurate at these lower values since this is where the majority of the motors are situated. For this reason weights have been assigned to the data points. The weights are assigned

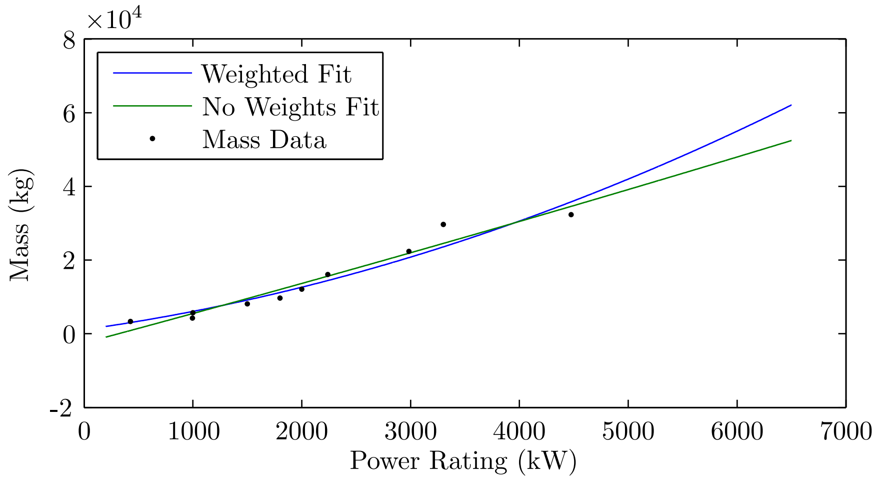

(a) Mass Fit

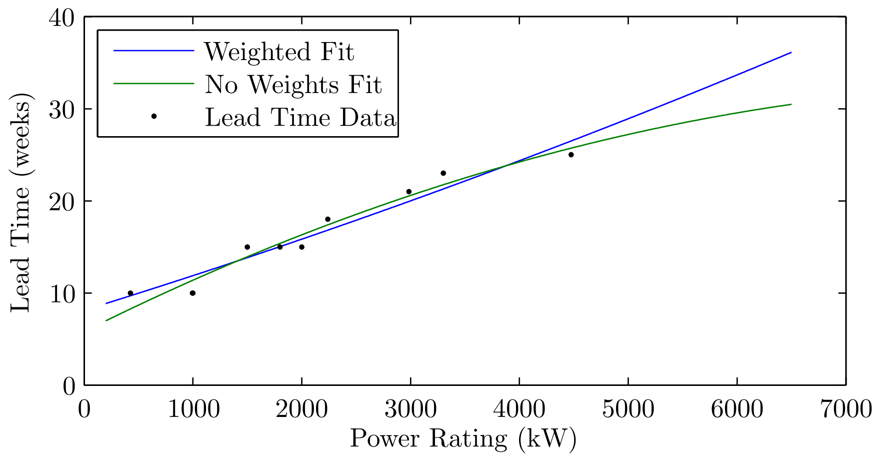

(b) Lead Time Fit

Figure 2.6: Mass and Lead Time Least Squares Fit

to be proportional to the number of motors which are represented by the point.

Let us start with the 138 motors in Class A (200 kW to 720 kW). Only the first point in table 2.5 falls in that range, and we must take all Class A motors into account. The next three points fall in the range of Class B, so the 30 Class B motors are evenly distributed over those points (10 each). The 66 Class C motors and the 19 Class D motors are used to assign weights in the same way. Note that three of the points fall in the range of both Class B & C, and will therefore receive weights from both. Weighting the points like this ensure that the fit is most accurate in the regions where the bulk of the motors lie.

Another solution to the problem would have been to force the curve to pass through the origin, however forcing this restriction reduces the accuracy of the fit in other parts.

2.6.2 Dividing the Total Embodied Energy

A weighted average is used to divide the total embodied energy among each of the motors.

The embodied energy of individual motors can now be determined:

$$E_{mass}\left(X_n\right) = \frac{mass\left(X_n\right)}{\sum mass\left(X_n\right)} E_{m_{tot}}\left(X_n\right) \tag{2.17}$$

$$E_{time}\left(X_n\right) = \frac{time\left(X_n\right)}{\sum time\left(X_n\right)} E_{t_{tot}}\left(X_n\right) \tag{2.18}$$

$$E\left(X_n\right) = E_{mass}\left(X_n\right) + E_{time}\left(X_n\right) \tag{2.19}$$

where

X_n = The power rating of a particular motor in the list of motors

E_{mass} = The raw materials component of the embodied energy of a particular motor

E_{time} = The electricity and gas component of the embodied energy of a particular motor

E = The total embodied energy of a particular motor

$mass$ = The mass of a particular motor

$time$ = The lead time of a particular motor

$E_{m_{tot}}$ = The total raw materials component of embodied energy

$E_{t_{tot}}$ = The total electricity and gas component of embodied energy

Figure 2.7 shows the embodied energy as a function of motor power rating for each of the four functions (equations 2.5 to 2.8). The hyperbolic tangent and exponential distributions generated almost identical embodied energy results. The impulse distribution is a close match but for far less effort. Finally the uniform distribution yields a different curve from the others. Since it neglects to take into account that the average power rating for a particular group of motors, the uniform distribution is not recommended. The

Table 2.6 shows the embodied energy for various motors power ratings (using the hyperbolic tangent distribution).

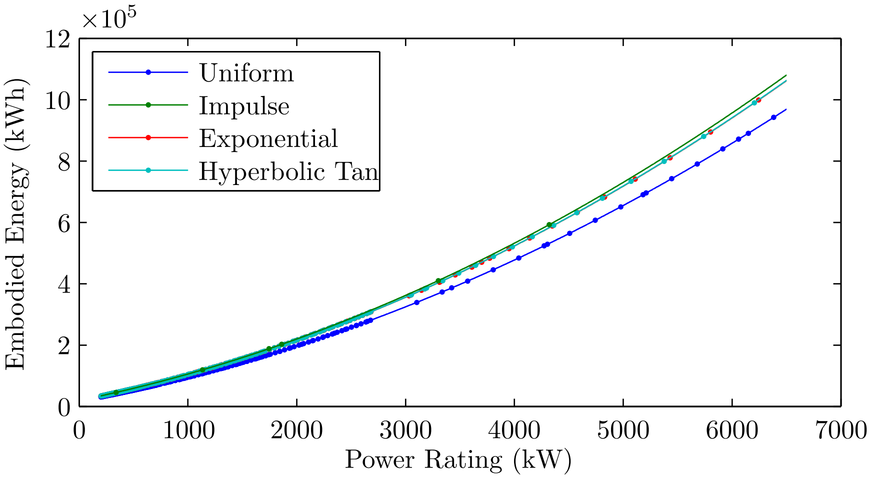

(a) Steel and Copper Component

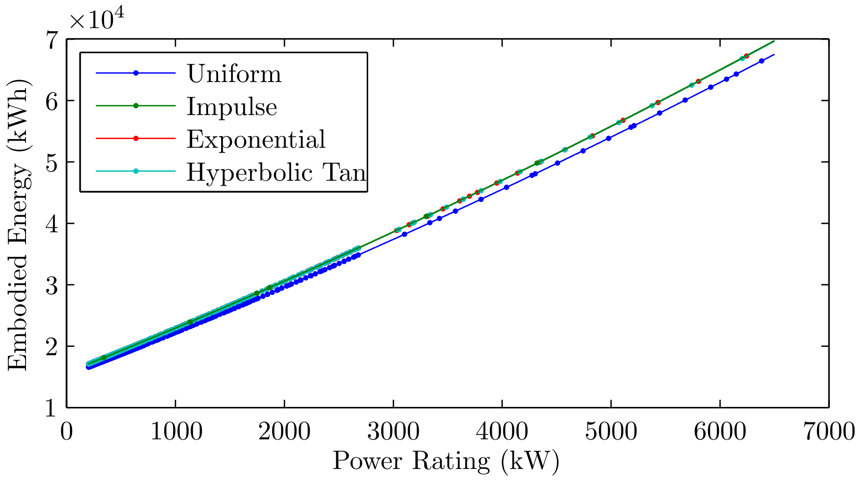

(b) Electricity and Gas

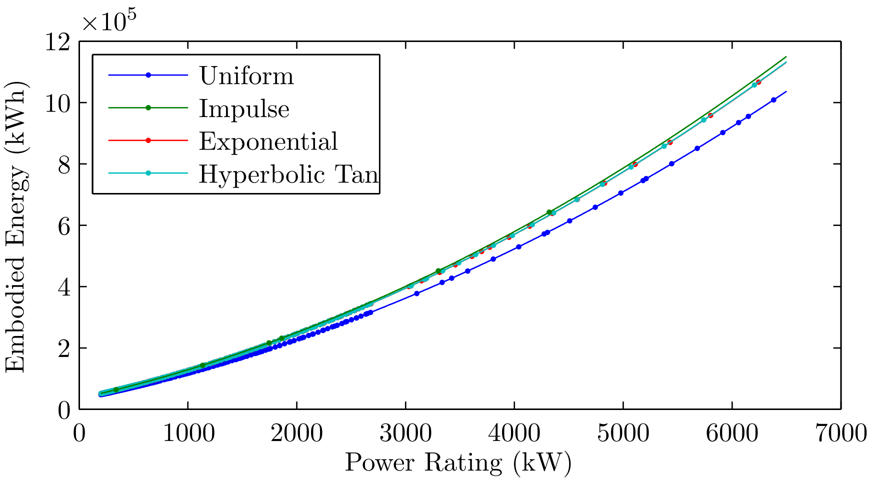

(c) Total

Figure 2.7: Embodied Energy as a Function of Motor Power Rating

Table 2.6: Embodied Energy versus Power Rating

Motor Power Rating kW	**Motor Embodied Energy** kWh
200	50 956
1 000	126 750
3 000	394 530
6 500	1 132 200

2.7 Analysis of Results

This investigation only covers motors in the Range from 200 kW to 6 500 kW. Great care should be taken when extrapolating to find the embodied energy of motors outside this range. This is especially true for smaller motors where the manufacturing processes may differ significantly for motors which are mass produced.

The results above only take into account the steel, copper, electricity and gas components of the embodied energy. Perhaps the estimate could be improved by taking into account some of the other materials. Additionally the embodied energy values for the steel and copper play a large role in in determining the total embodied energy of the motor, therefore these values should be as accurate as possible. The estimates for these embodied energies were all taken in an architectural content, and therefore the higher grades of steel used in motor laminations may have higher embodied energy. It may also be worth considering the fact that the motors use different grades of steel for different parts of the motor. Embodied energy of the raw materials may also differ slightly in different countries. Incorporating these suggestions should improve the accuracy of the estimates, but may require extensive further research.

The mass and lead time data given in table 2.5 plays a large role in determining the slope and shape of the curves in figure 2.7. Therefore getting a more accurate estimates of these values would also improve the estimate. Since a motor could spend 90% of the lead time in a badly managed process gathering dust, it is actually only the manufacturing time that contributes significantly to the embodied energy rather than the lead time. This data is however difficult to get without working inside the factory, and tracking the progress of each individual motor. If the ratio of the manufacturing time to the lead time is approximately constant for each motor then the current method will give identical results.

2.8 Conclusion

Although further research could be done to refine the embodied energy coefficients of the raw materials, and perhaps break the motors down into more subcategories rather than just copper and steel, this chapter describes a method that could be used in order to evaluate the embodied energy of various different electric motors.

Chapter 3

Pumping Efficiency Tests

This chapter details the small scale efficiency tests conducted. The aim was to check the difference in system efficiency between a standard and an energy efficient motor. The tests involved pumping water to different head pressures ranging from about 0.7 m to 8.0 m using a centrifugal pump. Two 0.37 kW three–phase induction motors from Siemens were used, an energy efficient motor and a standard motor.

For comparison the water flow rates are controlled using both a ball valve and a Variable Speed Drive (VSD). Each test was performed twice, once with the standard motor and once with the energy efficient motor. The results were compared in order to determine what energy savings could be expected between the two motors and the different flow rate control strategies.

Additionally since we were not only concerned with the system efficiency, many intermediate measurements were taken. We were thus able to determine the efficiency at each stage of the energy conversion process. The efficiency of the motor, pump, VSD as well as friction losses in the pipes and valve were all separately measured and investigated.

3.1 Stages of Energy Transfer

In order to find out the average efficiency of the whole system, or of the individual parts, it was necessary to calculate the amount of energy or power that was transferred through the system. The following equations describe the energy at various stages in the system:

Equation 3.1 describes the three–phase electrical energy supplying the VSD and motor [14].

$$E_{elec} = \int_0^T V \cdot I \, dt \tag{3.1}$$

where
E_{elec} = Electrical Energy (J)
V = Vector of Phase Voltages (V)
I = Vector of Phase Currents (A)

The motor converts electrical energy to rotational mechanical energy. The torque reading was measured by mounting the motor on a cradle with a load cell. The load cell measured the reaction torque from the motor (see appendix A for more details). Equation 3.2 describes the rotational mechanical energy at the output of the motor's gearbox and input to the pump [14].

$$E_{mech} = \int_0^T \tau \, \omega \, dt \tag{3.2}$$

where
E_{mech} = Mechanical Rotational Energy (J)
τ = Torque on the Shaft (N.m)
ω = Angular Velocity of the Shaft (rad/s)

A centrifugal water pump converts the mechanical energy into hydrodynamic (kinetic) energy. This energy was determined by measuring the flow rate and differential pressure of the water as it is pumped. The differential pressure is the difference in pressure at the inlet and outlet of the pump. In order to account for Bernoulli's principle (equation 3.3), both measurements need to be performed at the same level and the suction and discharge bore should be the same. A differential pressure gauge was however not available, so the pressure at the suction side of the pump was taken into account by monitoring the level of the supply tank and and the flow velocity. Equation 3.4 describes the hydrodynamic energy of the water being pumped [14]. This assumes that water is incompressible.

$$\frac{1}{2} \rho \, v^2 + \rho \, g_0 \, h + P = constant \tag{3.3}$$

where

ρ = Density of Water = 998.2 kg/m^3
v = Velocity of the Flowing Water (m/s)
g_0 = Free-fall Acceleration = 9.81 m/s^2
h = Height of the Point Above a Reference Plane (m)
P = Pressure at the Point (Pa)

$$E_{hydro} = \int_0^T P\,Q\,dt \tag{3.4}$$

where
E_{hydro} = Hydrodynamic Energy of the Water (J)
P = Differential Pressure (Pa)
Q = Flow Rate of the Water (m^3/s)

The system output is the gain in potential energy of the water after being pumped up the flight of stairs. Equation 3.5 describes the gain in potential energy of the water [14].

$$E_{pot} = V\ h\ \rho\ g_0 \tag{3.5}$$

where
E_{pot} = Potential Energy (J)
V = Volume of Water Pumped (m^3)
h = Pumping Head (m)
ρ = Density of Water = 998.2 kg/m^3
g_0 = Free-fall Acceleration = 9.81 m/s^2

Finally the efficiency of the whole system and its parts was determined by the equation 3.6. Usually efficiency is calculated using the instantaneous power rather than energy, however this equation will give the average efficiency for the test.

$$\eta = \frac{E_{out}}{E_{in}} \times 100\% \tag{3.6}$$

where
η = Average Efficiency
E_{out} = Output Energy (J)
E_{in} = Input Energy (J)

3.2 Test Setup

The schematic shown in figure 3.1 illustrates the experimental setup used for the measurements.

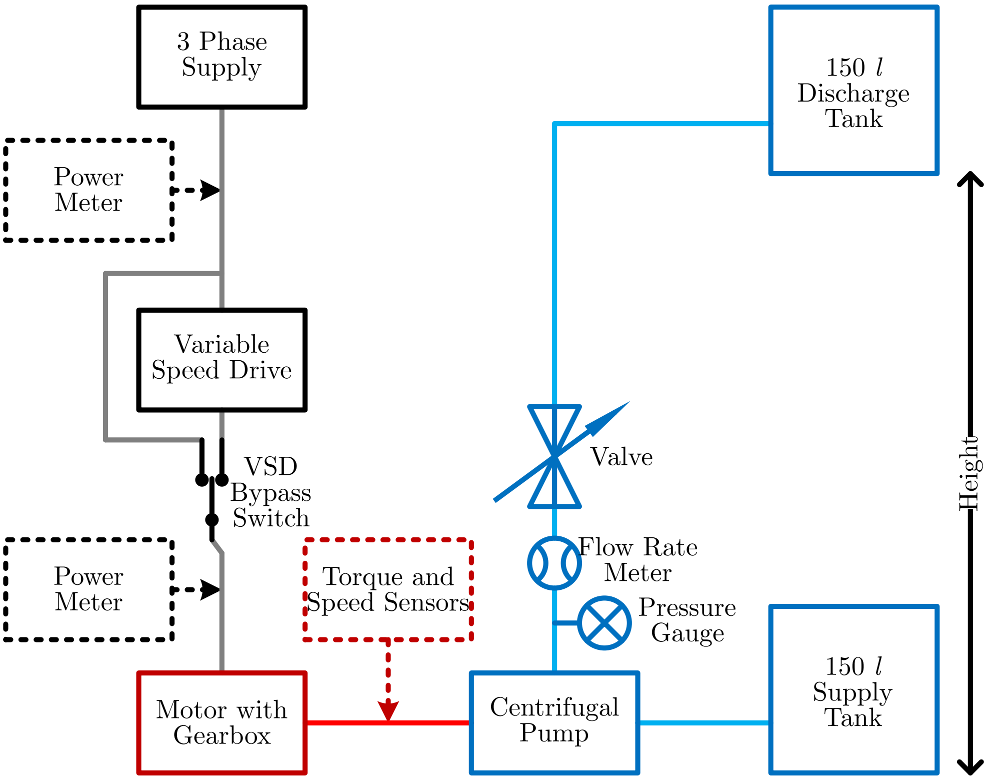

Figure 3.1: Experimental Setup Schematic

3.2.1 System Components

Table 3.1: List of system components

Item	Specification
Centrifugal Pump [15] (NT25–160)	Manufacturer: Rapid Allweiler Impeller Diameter: 159 mm Maximum Efficiency: 53%

Item	**Specification**
Energy Efficient Motor (1LA9070-2KA10–Z)	Manufacturer: Siemens Rated Frequency: 50 Hz Rated Power: 0.37 kW Power Factor: 0.77 Rated Voltage: 400/230 V Rated Current: 1.63/0.94 A Rated Speed: 2840 RPM Rated Efficiency: 74%
Standard Motor (1LA9070–2KA10–Z)	Manufacturer: Siemens Rated Frequency: 50 Hz Rated Power: 0.37 kW Power Factor: 0.81 Rated Voltage: 400/230 V Rated Current: 1.74/1.0 A Rated Speed: 2740 RPM Rated Efficiency: 66%
Gearbox (0707–M26882)	Manufacturer: Flender RSA Ratio: 1.85:1 One coupled to each motor.
Digital Power Meter (WT1600)	Manufacturer: Yokogawa
Clamp-on Power Meter (CW240)	Manufacturer: Yokogawa
Data Acquisition/Switch Unit (34970A)	Manufacturer: Agilent
Flow Rate Meter (transducer and computer) (SITRANS FM MAGFLO MAG5000) (SITRANS FM MAGFLO MAG5100 W)	Manufacturer: Siemens
Pressure Gauge (SITRANS P 7MF4033)	Manufacturer: Siemens

Item	Specification
Variable Speed Drive (Micromaster 440 6SE6440–2UD13–7AA1)	Manufacturer: Siemens Motor: 0.37 kW Input: 380–480 V 3Φ AC 2.2 A 47–63 Hz Output: 380–Input V 3Φ AC 1.2 A 0–650 Hz
Digital Photo Tachometer (RM–1501)	Manufacturer: Prova
Load Cell (1004)	Manufacturer: Tedea–Huntleigh Rated Capacity: 1.5 kg Total Error: 0.1 g
Ball Valve	
Clear Plasticised PVC Piping	Length: 30 m Inside Bore: 25 mm

3.3 Testing procedure

The investigation involves pumping 120 l of water up a flight of stairs. The discharge tank could be moved to different levels on the staircase to provide a variable static head. At each level various tests were performed by changing the power supply, changing the throttling of the valve and switching between the standard and energy efficient motors.

The tests were performed with the following head 7.97 m, 6.51 m, 5.07 m, 3.62 m, 2.17 m and 0.72 m. When changing the power supply, the motors were initially run directly from the three–phase incoming mains, and then from the VSD starting at 60 Hz and reducing the frequency in steps of 10 Hz until the motors were running too slowly to pump the water up the stairs. The valve was switched between fully open (0°) and half open (45°) for each of the above tests. Each of these tests was done using both the standard and the energy efficient motors. This resulted in a total of 96 tests. Unfortunately we forgot to set the valve for the final test, so only 95 sets of results are given in appendix D

For each test the voltage, current, power, energy, power factor, torque, angular velocity, pressure, flow rate, volume pumped and various other readings were sampled and logged.

3.4 Torque Reading Errors

After taking the whole set of readings we noticed that the torque measurements were not sufficiently accurate to calculate the mechanical power at the output of the motor's gearbox and input to the pump. The measured torque offset before and after the tests would often differ considerably, as show by figure A.2. Since the load cell in isolation had a relatively small hysteresis, we can conclude that the friction in the bearings of the torque measurement rig were the problem. While other solutions are available – in-line rotary torque sensors being the most common – these sensors can be rather costly, which is part of the reason for avoiding them in the first place. The design of the torque measurement rig is described in appendix A.

While ideally we would have like to accurately measure the torque, it was not too difficult to estimate. The two motors were be modelled fairly easily, and torque–speed curves were developed for each (see appendix B for more details). Since the input voltages and currents as well as the output angular velocities have been measured, the torque could easily be read off the corresponding torque–speed curve of the motor model.

This problem can also be tackled from the viewpoint of the pump. The pump data sheet specifies the pump efficiency for different operating conditions (see appendix C for more details). Since the differential pressure, flow rate and angular velocity of the pump were accurately measured, we were able to find the input power and therefore torque for those conditions from the data sheet.

Having estimated the torque using both methods, using the pump curves seemed to give more reliable results. The motor model seemed to predict higher currents than those measured in table D.2. This was especially true at the lower frequencies. The model therefore overestimated the output power of the motor (for a given voltage, frequency and slip). This may have been due to the fact that the no load and locked rotor tests used to predict the motor model were performed using a generator set with low harmonics while the actual pumping tests used a VSD. On the other hand, the predictions made by equation C.1 were as expected. The rated efficiency of the energy efficient motor is 66% and the predicted efficiency of the pumping tests ranged from 55% to 37% which seemed reasonable.

3.5 Results

A total of 96 different tests were performed (unfortunately for the last test the valve was in the wrong position). These include both motors, different degrees of throttling with the valve, different static heads, different VSD frequencies or bypassing the VSD and operating the motor directly from mains. The results have been tabulated in appendix D.

3.5.1 Efficiency of the Variable Speed Drive

The variable speed drive is specified to have an efficiency between 96% and 97%. The results from table D.1 show the measured VSD efficiencies ranging from 90.7% to 98.9%. At higher frequencies the VSD was more efficient than at lower frequencies, however this is likely due to the fact that the motor operated with a poor power factor at low frequencies. Despite this the VSD is by far the most efficient part of the entire system.

3.5.2 Efficiency of the Motors

The efficiency of the motors range from 35% to 55%, and efficiency improvements of between 1% and 6% were evident between the standard and energy efficient motors. These efficiency improvements amounts to power saving of about 15 W between the two motors, however it differs between tests.

3.5.3 Losses in the Gearbox

Neither the gearbox input or output power have been measured, however the motor output power with and without the gearbox was predicted in figure B.5. Gearbox losses make up the difference between the two curves. A second order polynomial was used to describe the gearbox friction and is given by equation 3.7 and figure 3.2.

$$Fr = 7.788{\times}10^{-4}\,\omega^2 + 2.139{\times}10^{-1}\,\omega + 2.878{\times}10^{-2} \tag{3.7}$$

where

Fr = Friction Loss in the Gearbox (W)

ω = Angular Velocity at output of Gearbox (rad/s)

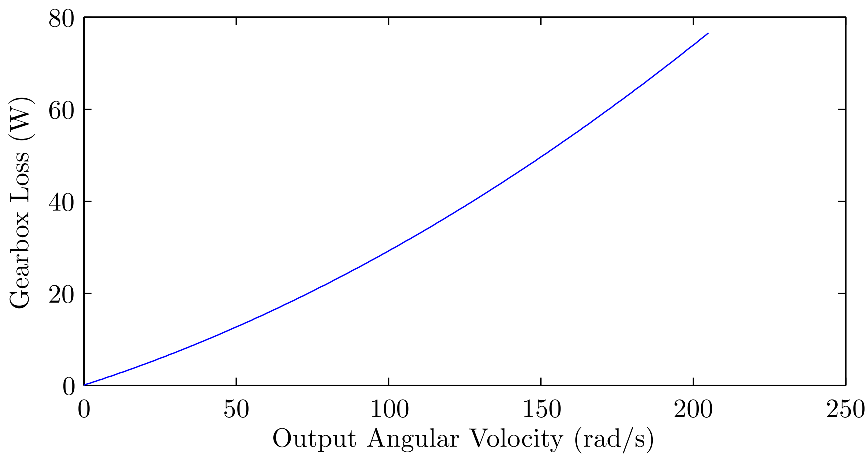

Figure 3.2: Losses in the Gearbox versus Angular Velocity

The gearbox steps down the angular velocity (and steps up the torque) with a gear ratio of 1.85:1. Considering the the rated power of the motor is only 370 W (at a gearbox output angular velocity of about 160 rad/s), there is a fairly significant power loss associated with the gearbox. Since the efficiency of a 4–pole motor is about the same as a 2–pole motor (possibly slightly more efficient [4, 5]), the use of a gearbox may not be justifiable at all. By using a 4–pole motor rather than a 2–pole motor the gearbox may be removed altogether, with a minor change in angular velocity (ratio of 2:1 rather than 1.85:1). Perhaps in some instances an exact angular velocity may be required, but when operating the motor with a VSD this arguement becomes very difficult.

3.5.4 Efficiency of the Pump

The top part of figure C.1 gives the characteristic curves for the pump, which show a relationship between the pressure, flow rate, angular velocity and pump efficiency. By plotting the efficiency as a function of both pressure and flow rate, we can compare the test results to the data sheet. The pressure and flow rate have been converted to the same units as the data sheet, so that they can easily be compared. As expected the measured values of (figure 3.3) closely correlate with the data sheet (figure C.1).

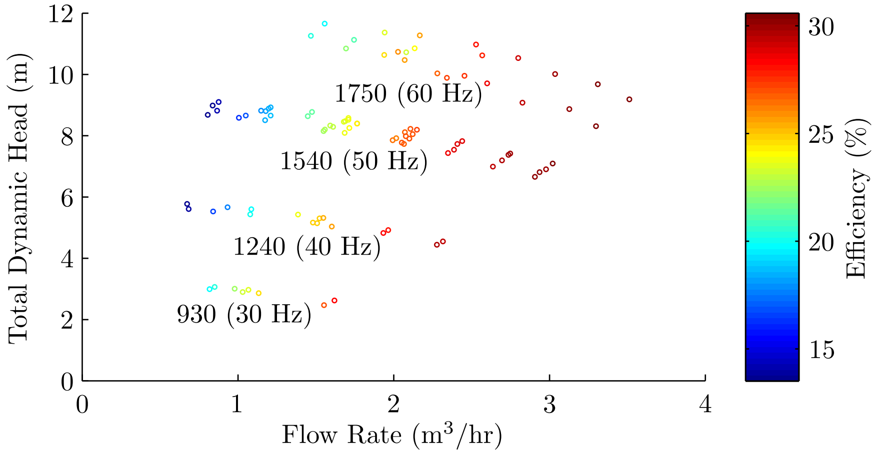

Figure 3.3: Efficiency of the Pump versus Flow Rate and Pressure

It is clear that the the pump is not operating at optimum efficiency. The data sheet suggests that at a particular angular velocity, the efficiency of the pump increases with increased flow rates and reduced pressures. The use of a valve to control flow rate clearly does the exact opposite, and thus reduces the efficiency of the pump.

3.5.5 Losses in the Pipes and Valve

The pump produces the hydrodynamic power of the flowing water. This water then flows through the piping and valve where it is converted to potential energy. There are some losses in the system mostly due to friction and turbulence in the piping and valve. Figure 3.4 shows that this loss is related to the flow rate. With the valve open, the points seem to all lie an the same line, while with the valve at 45° the points are more scattered. This can be easily explained since the position of the valve was simply estimated by hand, and was not necessarily at exactly the same position for each test.

It can immediately be seen in figure 3.4 that with the valve at 45° the dynamic flow losses are greater at every flow rate than with the valve fully open. Therefore another means of controlling the flow rate such as a VSD should be seriously considered.

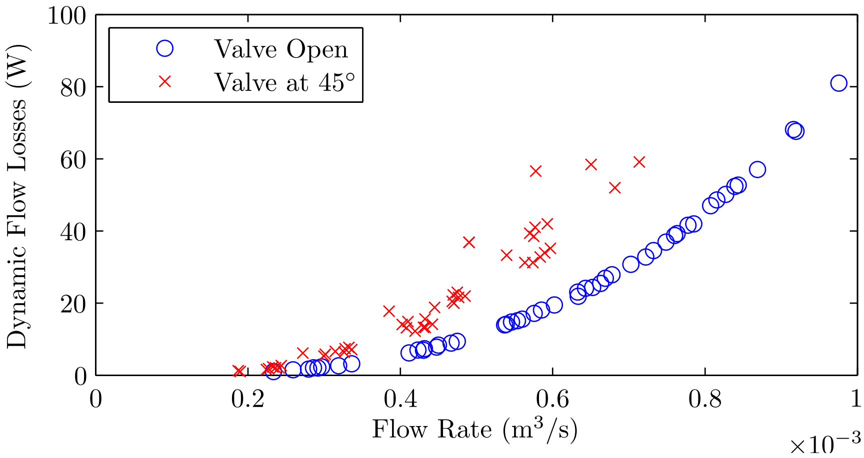

Figure 3.4: Dynamic Flow Losses versus Flow Rate

These tests all used a ball valve, and although other valves may create less turbulence and therefore be more efficient, that has not been investigated in this research.

The pumping pressure needs to overcome the static head and the dynamic flow losses. In order to increase the flow rate, the pressure must increase as well. It therefore follows that the dynamic losses increase with flow rate (for a particular valve position). Thus the efficiency of the pipe and valve subsystem will be higher at at lower flow rates. Additionally the ratio of dynamic flow losses to static head decreases as the static head is increased. So the efficiency of the pipe and valve increases with increasing static head and decreasing flow rate.

The efficiency of the pump increases with increasing flow rate and decreasing pressure, and the efficiency of the pipe and valve increases with decreasing flow and increasing pressure. Therefore (for a given pipe and valve configuration) there will be an optimal pressure and flow rate which maximises the efficiency of the combination (pump, pipe and valve).

3.5.6 The Overall System

Finding the efficiency of the intermediate subsystems increase understanding, and help to improve the efficiency of each. However it is the efficiency of the entire system which one really wants to maximise. This subsection looks at the system efficiency for different conditions.

System Efficiency versus Flow Rate

Figures 3.5 to 3.10 show the average system efficiency as a function of flow rate and supply frequency with the discharge tanks at each of the six different levels. In each figure the solid lines represent the efficiency when using the energy efficient motor, while the dashed lines represent the efficiency when using the standard motor. The lines moving outwards from the origin represent the efficiency and flow rates that would be expected if a valve is used to control the flow rate (at each frequency). The *horizontal* lines show he expected efficiency and flow rates when using the VSD to control flow rate at (each valve position).

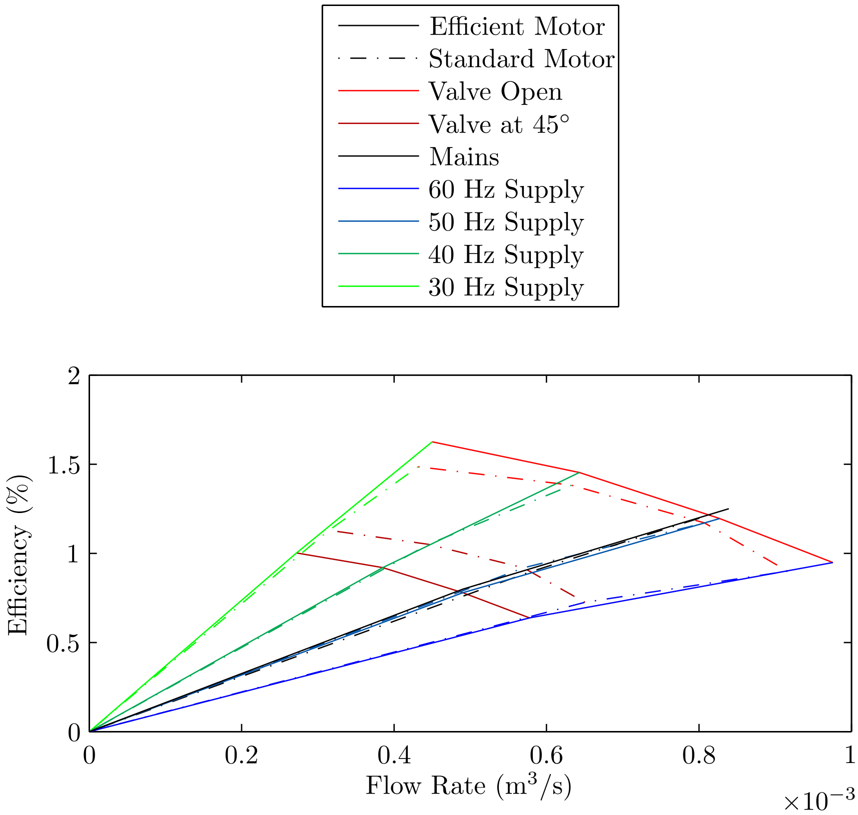

Figure 3.5: System Efficiency versus Flow Rate with a Static Head of 0.72 m (with Legend)

The results when using the VSD at 50 Hz and when supplying the motor directly with mains were similar but as expected the efficiency when using mains directly was higher. This was mostly be due to the VSD losses and (to a lesser extent) increased losses in the motor as a result of the harmonics generated by the VSD.

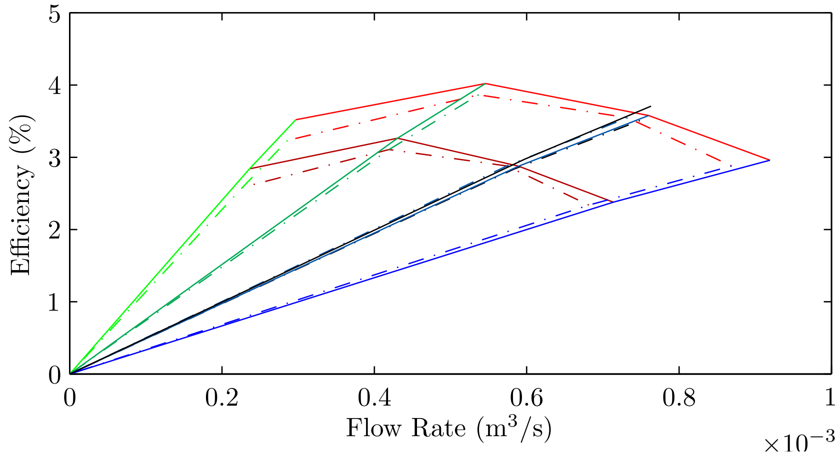

Figure 3.6: System Efficiency versus Flow Rate with a Static Head of 2.17 m

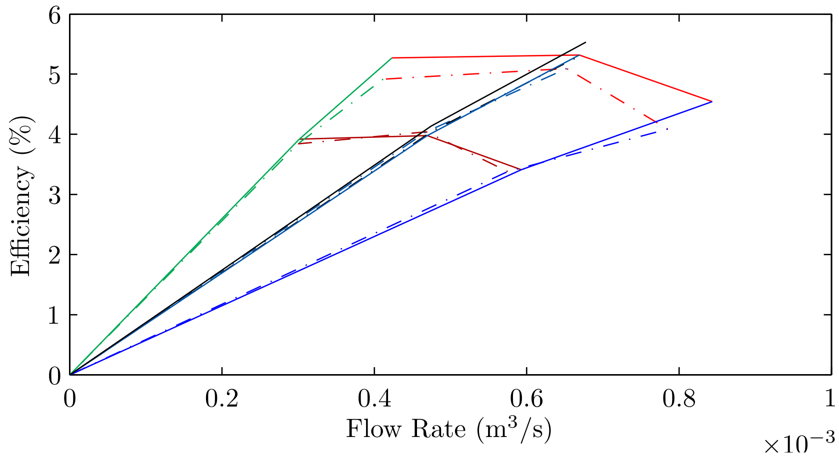

Figure 3.7: System Efficiency versus Flow Rate with a Static Head of 3.62 m

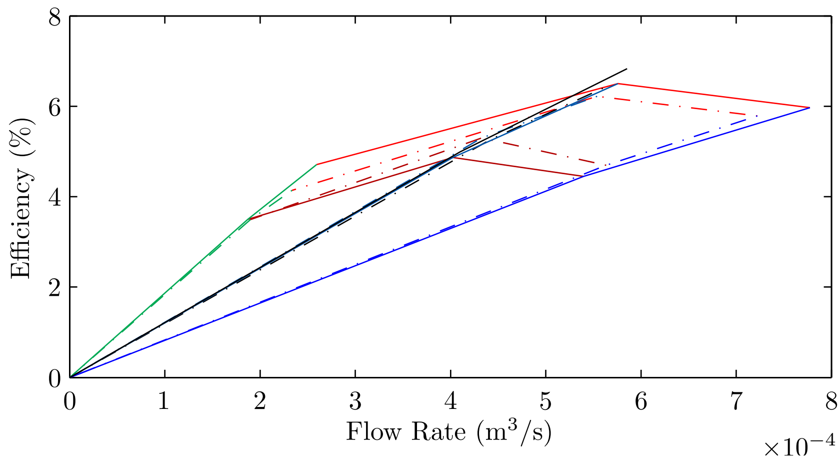

Figure 3.8: System Efficiency versus Flow Rate with a Static Head of 5.07 m

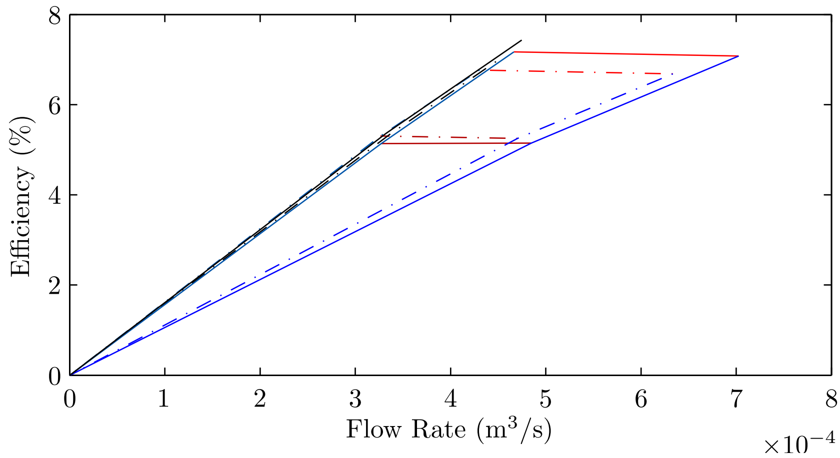

Figure 3.9: System Efficiency versus Flow Rate with a Static Head of 6.51 m

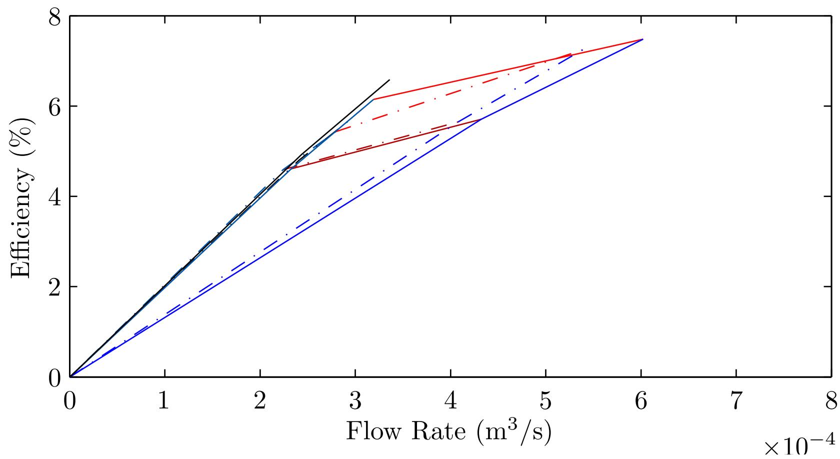

Figure 3.10: System Efficiency versus Flow Rate with a Static Head of 7.97 m

Clearly the system efficiency decreased when the valve was used to control the flow rate, and although a valve is the easiest way to control the flow rate, it comes at the cost of efficiency. On the other hand the efficiency is far more constant when using the VSD. It is also evident that the efficiency can actually also be improved by using a VSD and operating at the optimal frequency rather than simply supplying the motor from mains.

Finally although the energy efficient motor offers a better system efficiency than the standard motor (as expected), these efficiency improvements are not particularly large. In figure 3.5, the efficiency of the standard motor seems to be higher than the energy efficient motor with the valve at 45°, however this is simple due to the fact valves were not at the exact same position when the two motors were being tested.

System Efficiency versus Static Head

This time we show that for different VSD frequencies the head at which maximum system efficiency occurs differs.

Figures 3.11 to 3.15 show that the static head at which, maximum efficiency occurs varies with frequency. For a system where the static head changes, the motor supply frequency which the system is most efficient varies. A VSD could be used in order to continously operate the motor at the optimum frequency for each static head.

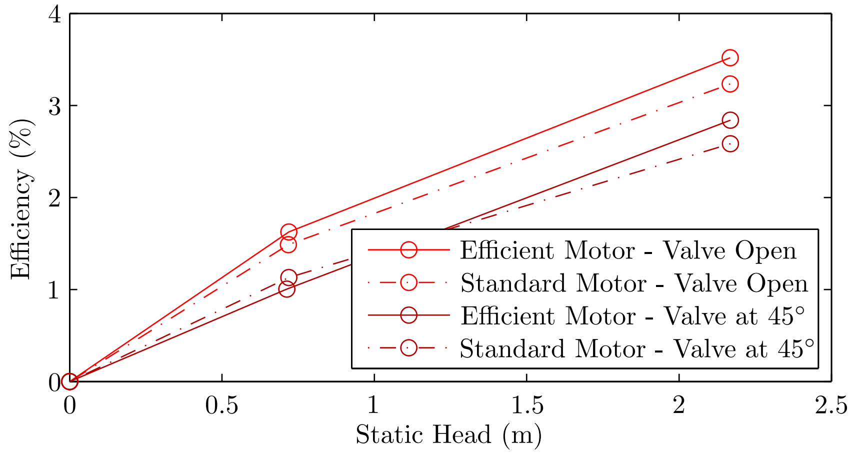

Figure 3.11: System Efficiency versus Static Head supplying the Motors at 30 Hz

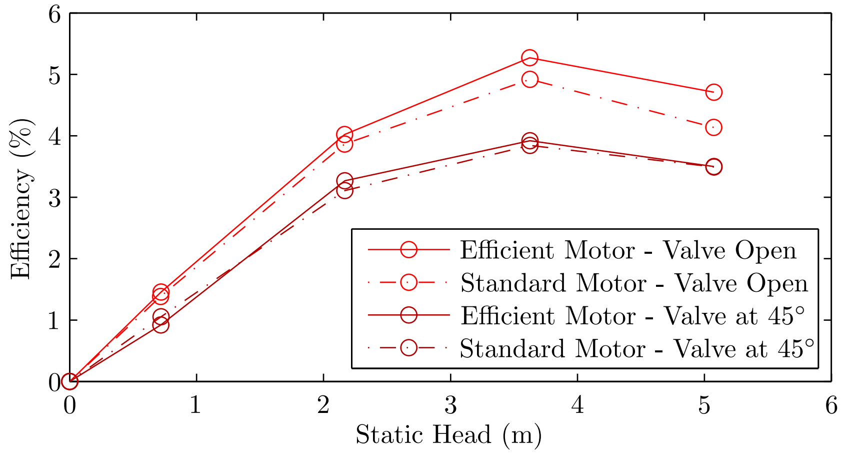

Figure 3.12: System Efficiency versus Static Head supplying the Motors at 40 Hz

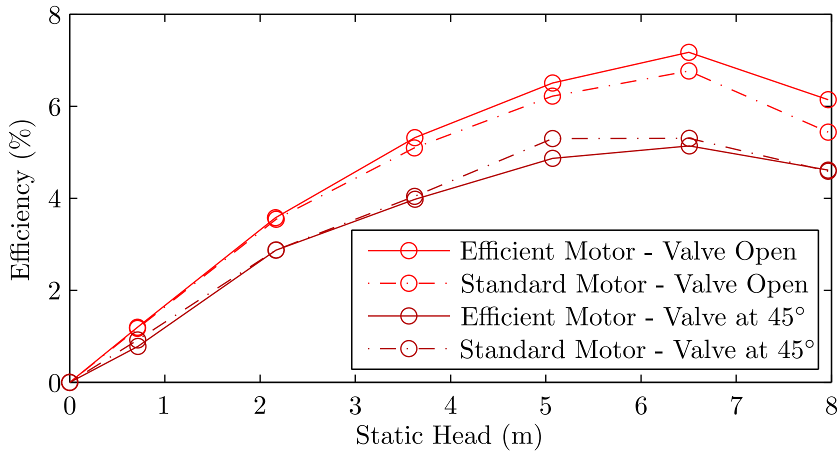

Figure 3.13: System Efficiency versus Static Head supplying the Motors at 50 Hz

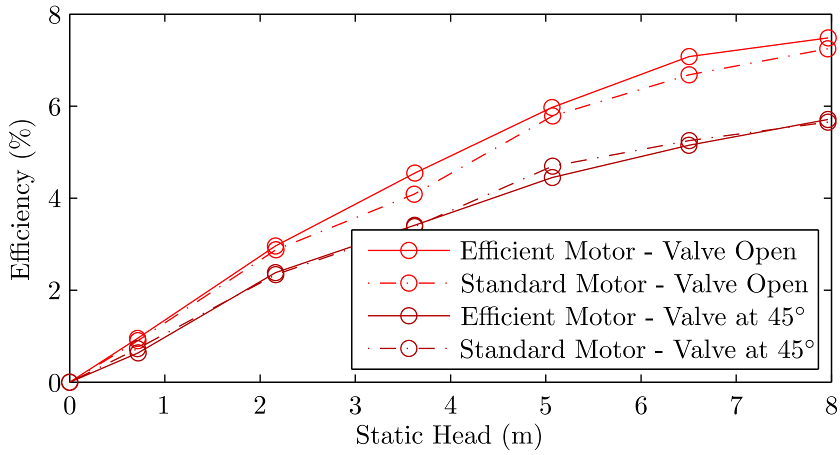

Figure 3.14: System Efficiency versus Static Head supplying the Motors at 60 Hz

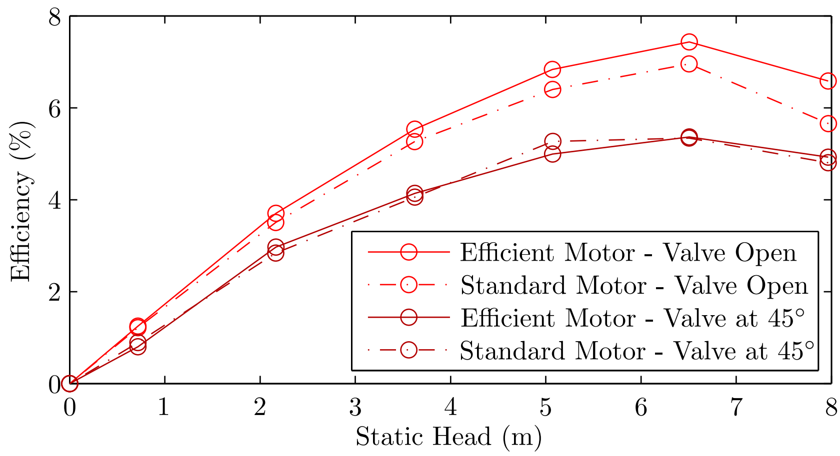

Figure 3.15: System Efficiency versus Static Head supplying the Motors with Mains

3.6 Discussion

3.6.1 Energy Efficient Motor or VSD?

"The pump-turbines used in Eskom's two pumped storage schemes at Drakensberg and Palmiet provide average generating and pumping efficiencies of over 90% and total cycle efficiencies of 73.7% at Drakensberg and 77.9% at Palmiet" [16]. By comparison, with the experimental system efficiency peaking at around 7%, it is certainly evident that it is not very efficient at all. Firstly it is noted that the system was never designed for maximum efficiency, and secondly we only used off the shelf equipment which was available in the lab. Also, since the pumping is done on a small scale, we would expect the efficiency to be significantly lower than a large industrial setup.

There are certain changes that could be made to improve the system efficiency. Obviously upgrading from a standard motor to an energy efficient motor will result in an improvement, however the efficiency improvement is small. Other solutions may yield greater efficiency improvements.

If we consider the system using the standard motor connected directly to the grid and using a valve to control flow rate, we have two main choices: *(i)* keep the same motor, but remove the valve and rather use a VSD to control the flow rate; or *(ii)* keep the valve and continue to operate the motor with mains, but upgrade the motor to an energy efficient motor. The efficiency gains from the energy efficient motor are insignificant in comparison to the loses of the valve, therefore *(i)* would be the better choice. In reality most ground water systems simply use a valve to control the flow rate. Even if flow rate control is not important, the tests show that installing a VSD and operating the motor at frequencies other than 50 Hz may also improve the efficiency more than one could expect from upgrading to an energy efficient motor.

3.6.2 Soft Starting

The use of a VSD can also improve the starting characteristics of the motors. Direct on-line starting of the motors will result in high starting currents. This will lead to reduced efficiency, especially for a process which requires repeated starting and stopping. High starting currents and torque may increase the wear and tear on the motor. These problems may be reduced with a VSD.

3.6.3 Power Factor

Furthermore a VSD may be used to improve a poor power factor, however input power factor correction circuits are uncommon on VSDs as they typically increase costs and decrease efficiency [17]. In some special circumstances however it may be justifiable to use a VSD for power factor correction.

On the other hand it is more likely that the VSD uses a simple diode bridge to power the DC bus. This can result in poor power factor and large harmonics. This may result in harmonics being fed back onto the grid, and poor power quality. In the extreme case, it may even lead to grid instability.

3.7 Conclusion

For the scale investigated, a variable speed drive is clearly more efficient to a valve for controlling the flow rate. The results also show that the efficiency improvements that could be expected by installing a VSD on a standard motor are also far greater than those expected by upgrading to an energy efficiency motor and keeping the valve flow rate control. For a system where static head varies, a VSD may be used in order to always operate the motor at the optimal frequency.

A variable speed drive adds soft starting capabilities to the motor. This may further improve efficiency especially in an application where the pump is repeatedly switched on and off. Soft starting may also reduce the wear and tear on the system as it will reduce the high starting currents and torque.

Chapter 4

Energy Payback Period

We have shown that the there is an energy saving when upgrading from a standard motor to an energy efficient motor. However we have also shown that there is an upfront embodied energy which needs to be invested to manufacture the new motor. This chapter aims to combine the previous chapters, and estimate how long one would need to operate the new motor before the energy savings exceed the upfront embodied energy investment. We should also take into account the remaining useful life of the old motor, which is wasted when the motor is destroyed in the EEM programme.

One difficulty is that the embodied estimate calculations were performed on induction motors ranging from 200 kW to 6 500 kW, the pumping tests were performed with 0.37 kW induction motors, and the Eskom EEM programme is only covers motors in the range 1.1 kW to 90 kW. Clearly there is no overlap and extrapolations should be considered carefully, however with the resources available this was the best that could be done.

4.1 Extrapolating the Embodied Energy

The data in table 2.1 only covers motors ranging from 200 kW to 6 500 kW. We therefore should not use this data to make embodied energy predictions about motors outside this range. Ideally we should repeat the embodied energy estimate study for but with motors in the correct range.

If we simply extrapolate the curves from figure 2.7(c), we find that the embodied energy of a 0.1 kW motor is about 34 800 kWh (the y–intercept). Common sense should tell us that this estimate is too high, and that the embodied energy should approach zero as the motor power rating approaches zero. If on the other hand we fit a straight line from the origin to the embodied energy at 200 kW, then we have some difficulty explaining the sudden change in slope.

Smaller motors are usually mass produced and may therefore be manufactured more efficiently than larger motors. We may therefore even find a discontinuity in the embodied energy between the smaller motors which are mass produced and the larger motors which are custom made. The materials of these motors also change, the two 0.37 kW motors (which were used in in the pumping efficiency investigation) have an aluminium frame rather than a steel frame.

Figure 4.1 gives an upper and lower bound to use for the embodied energy of motors smaller than 200 kW. For a 90 kW motor, if we can accept that it is in the range from 23 000 kWh to 42 000 kWh, then at least the upper and lower bounds are within the same order of magnitude. On the other saying that a 0.37 kW motor has an embodied energy between 95 kWh and 34 800 kWh is not very helpful.

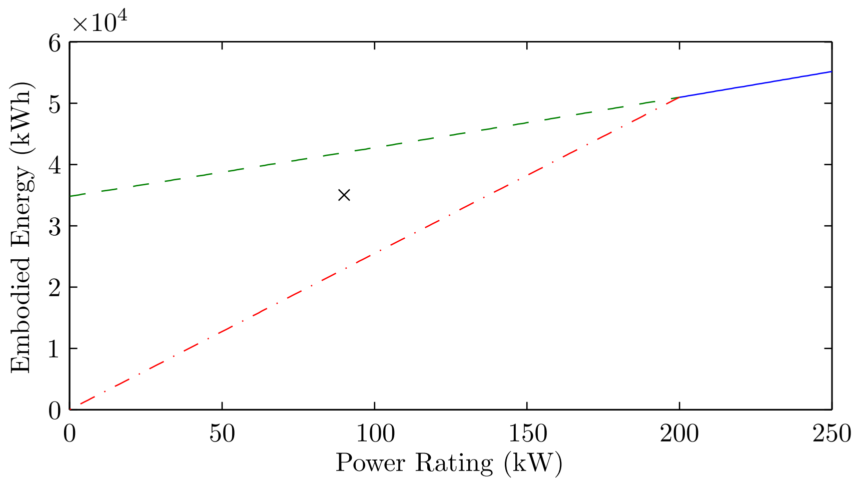

Figure 4.1: Extrapolating the Embodied Energy

4.2 Theoretical Payback Periods

The payback period is the amount of time that it would take for the energy savings of the replacement motor to cover the embodied energy of that motor. To calculate the energy savings we need to ensure that there is a common output between the two motors. Equations 4.1 to 4.3 show the payback period where each motor (or system) operates at the same output power, but with different efficiencies.

$$T = \frac{E}{P_{inold} - P_{innew}} \tag{4.1}$$

$$\eta = \frac{P_{out}}{P_{in}} \tag{4.2}$$

$$T = \frac{E}{P_{out}} \frac{\eta_{new}\, \eta_{old}}{\eta_{new} - \eta_{old}} \tag{4.3}$$

where

T = The energy payback period of the replacement motor (s)

E = The embodied energy of the replacement motor (J)

P_{in} = The input power of the motor at an output power P_{out} (W)

P_{out} = The common output power of both motors (W)

η = The efficiency of the motor at the specified output power

old = The old motor

new = The new/replacement motor

If we consider an example where we replace an old 90 kW motor with a new one. Let us assume that the new motor has a full load efficiency of 95% (the minimum of a 90 kW Eff1 motor) and an embodied energy of 35 000 kWh. Now the payback period will be a function of the efficiency of the old motor, and is given in figure 4.2. With an efficiency of 93.9% (the minimum efficiency of a 90 kW Eff2 motor) the payback period will be 31 500 hours. A payback period of 6 700 hours can be expected when the old motor has an efficiency of 90%. This represents about 3.6 years of continuous operation and 15.1 years operating at 40 hours per week.

4.3 Pump Setup Payback Period

In the pumping tests equation 4.3 is not applicable, since the the output power differs depending on which motor is used. In this case we should rather measure the difference in average input energy required per m^3 of water pumped. This is given by equation 4.4.

$$V = E \frac{V_{tank}}{E_{inold} - E_{innew}} \tag{4.4}$$

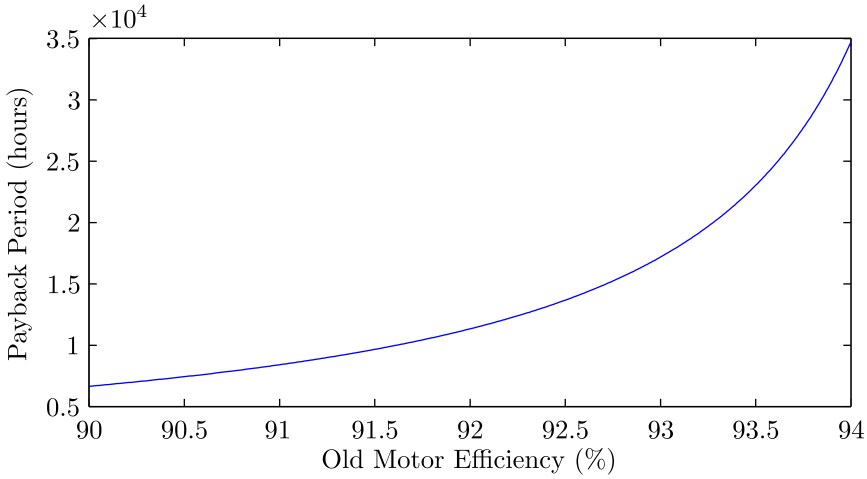

Figure 4.2: The Payback Period of a 90 kW Eff1 Motor

where

V = The amount of water which needs to be pumped before the embodied energy of the (m^3)

E = The embodied energy of the replacement motor (J)

V_{tank} = The volume pumped for the duration of the test (m^3)

E_{inold} = The input energy to pump a tank of water using the old motor (J)

E_{innew} = The input energy to pump a tank of water using the new/replacement motor (J)

The weight of the 0.37 kW motors is about 5 kg. Let us assume that the motor consists of 70% steel, 20% aluminium and 10% copper (by mass). Then taking into account only the raw materials portion of the embodied energy (from table 2.3, and using an embodied energy of 227 MJ/kg for aluminium [6, 8–10, 12]) we find that the embodied energy of the motor is about 104 kWh. Including manufacturing energy, let us assume an embodied energy of about 500 kWh.

To keep the table short and to the point, only the tests with the motors connected directly to the grid (no VSD) will be considered. Also the tests which had the valve at 45°, are not considered since the position of the valve may not have been at the exact same position for each test. Table 4.1 shows the volume of water that needs to be pumped at each height before new motor has repays its embodied energy. This is then converted to a payback period by taking into account the average flow rate for the test.

Table 4.1: Pump Setup Payback Period

Average Static Head m	**Payback Volume** m^3	**Payback Period** h
7.97	9 230	7 627
6.51	30 918	18 088
5.07	36 080	17 121
3.62	55 153	22 597
2.17	56 108	20 418
0.72	114 041	37 752

4.4 Discussion

Although more research may need to be performed to find better embodied energy estimates for motors smaller than 200 kW, this chapter suggests that a payback period of a few years can be expected when replacing an Eff2 motor with an Eff1 motor. To save energy it is best to take the motor with the highest efficiency, it may however not be wise to replace an existing functioning motor. In order to make that decision, you need to evaluate what efficiency improvement can be expected, how much embodied energy went manufacturing the new motor and finally how many hours the motor will be used in a typical year.

When we deal with finances, it is usual to have to pay back a debt with interest. Therefore a payment (or receipt) now is worth more than the same nominal amount in a years time, or worded differently, the present value of a payment now is higher than the present value of the same payment in a years time. Perhaps a similar approach should also be taken with the embodied energy. This would increase the payback periods, especially for motors which are not used frequently. Now a motor which is under utilised would never be worth replacing as it would not even pay back the *interest* on the embodied energy.

Clearly replacing an inefficient motor with a more efficient one may in fact use more energy than it saves.

Even if you can justify replacing an old motor with a more efficient one, it seems wasteful to destroy a perfectly good motor simply because it is slightly less efficient. Somebody else who would otherwise need to purchase a new motor at the expense of embodied energy could instead get *free* motor. Also with the planets limited raw materials, we should not take into account only the energy it takes to mine and process the the raw materials, but also the cost to the environment to waste the raw materials themselves. The following quotes: “the throwaway economy is on a collision course with the earth’s geological limits” and “assuming an annual 2% growth in extraction, U.S. Geological Survey data on current economically recoverable reserves show the world has 25 years of reserves for copper” [18] that the actual raw materials themselves are scare and wasting them has consequences for the environment.

4.5 Conclusion

This chapter unified two separate branches of the research. With the embodied energy and the efficiencies of the motors, one can make calculated decisions as to whether replacing an old motor will save or consume energy in the long run. Unfortunately the two branches of the research cover different motor power ratings. And therefore the payback periods should be taken under consideration.

The payback periods depend on the size and efficiencies of the old and new motors respectively. It also depends on how much the motor is used. However payback periods of between one and five years with continuous use should be expected (if we assume that there is no interest on the embodied energy). One should also consider the fact that the raw materials used to manufacture the motor themselves are scarce, and destroying a perfectly good motor to replace with a more efficient one is a wasteful use of the materials.

Appendix A

The Rig for Measuring Torque

A torque measurement rig is necessary to find measure the mechanical rotational power transferred from the motor to the pump. The design considerations for measuring the torque are given in this appendix.

A.1 The Design

A torque measurement rig was built, which measured the reaction torque on the stator of the motor. Newtons third law states, "if a force acts upon a body, then an equal and opposite force must act upon another body". Therefore measuring the reaction torque on the stator will be equal in magnitude to the torque on the shaft between the motor and the pump.

The test rig involved a cradle on which the motor and gearbox were mounted. With the cradle mounted on bearings (one connected to the pump, and the other to a vertical piece sicking up from the base), it is able to swing when subjected to a torque. A single load cell then measures the force exerted by the cradle, and can be converted to torque.

A the plan end elevation views of the torque measurement rig are given in figure A.1. The drawings are not to scale.

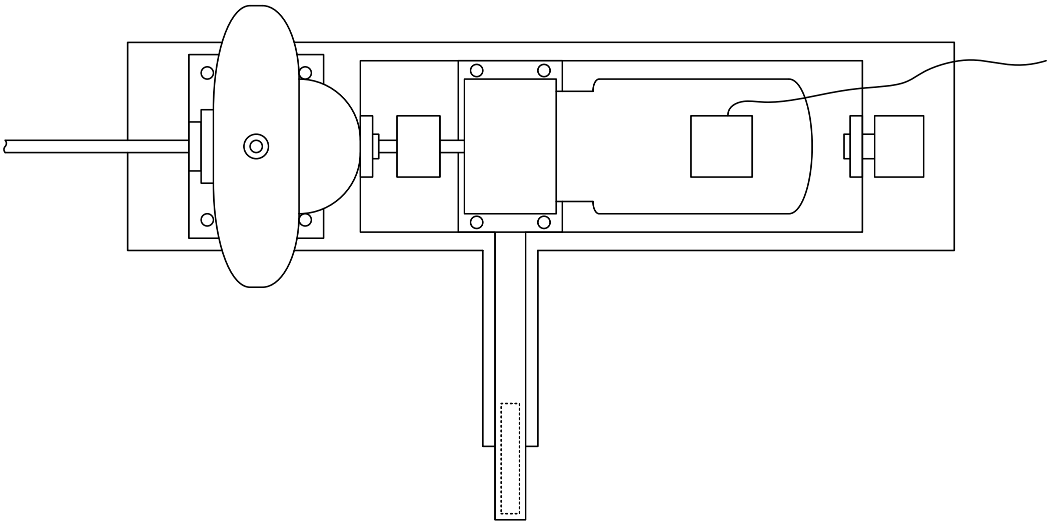

(a) Plan

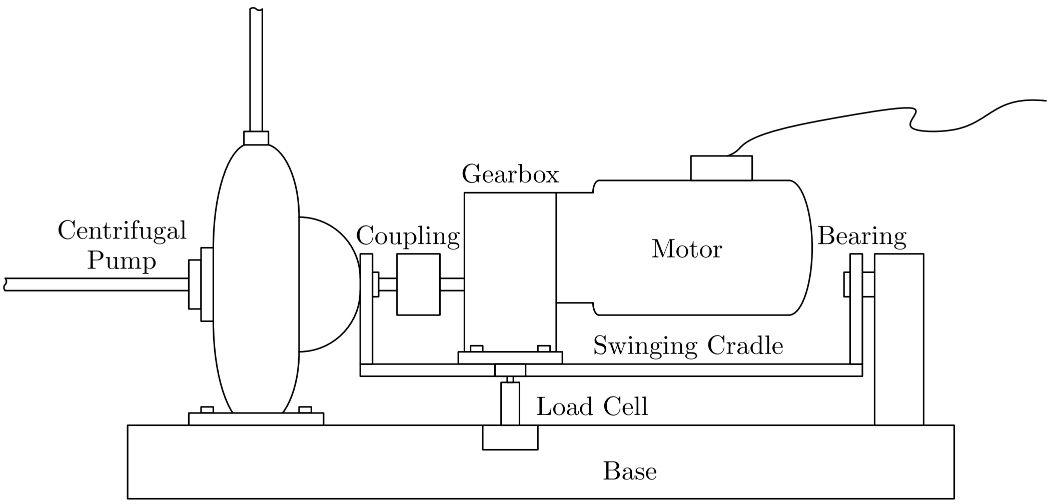

(b) Front Elevation

Figure A.1: Third Angle Projection of the Torque Measurement Rig

A.2 Calculations

The torque can be calculated from equation A.1.

$$\tau = F\,r \tag{A.1}$$

where

τ = The Reaction Torque Measured by the Rig (N.m)

F = The Force Measured by the Load Cell(N)

r = The Radius from the Center of the Rig to the Load Cell (0.426 m)

Gravity also acts on the cradle and motor, therefore for bottom heavy an additional torque (due to gravity) will keep the cradle centred. This means that any torque exerted by the motor will be required to overcome this torque before loading the load cell, and will result in errors in the readings. Hence care was taken to ensure that the the cradle with the motor was balanced.

A.3 Problems

The torque values proved to be much smaller than we were able to accurately measure. They peaked at about 1.2 N.m. Figure A.2 shows shows a graph of torque versus elapsed time for one of the tests. The difference in the offset before and after the test differed significantly (about 60% of full scale), and it is impossible to decide what the actual offset is. A load cell in isolation also exhibits this hysteresis, however this error was far beyond the specifications of the load cell. This suggests that friction in the bearings of the cradle was the problem. Although the rig should have worked in theory, in practice friction was a problem.

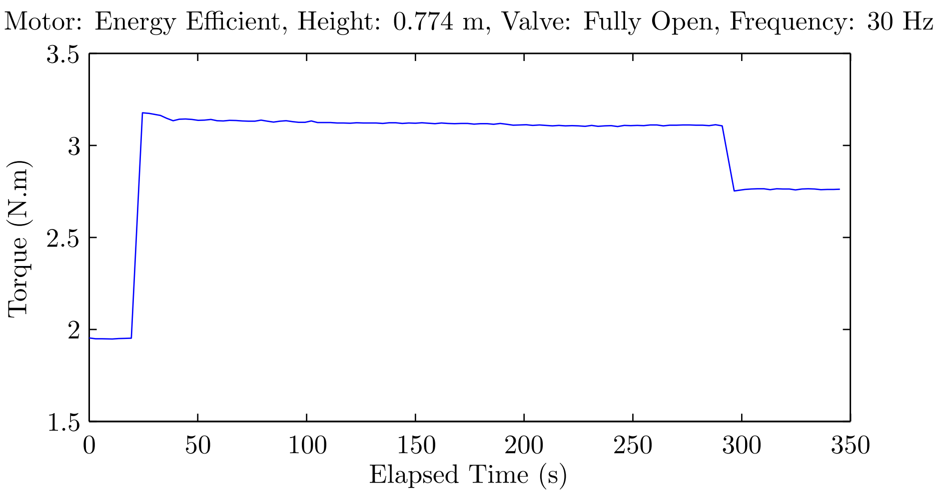

Figure A.2: Torque Measurement Errors due to Friction

It seems that the problem is friction in the bearings of the cradle. When a torque is applied, the cradle moves slightly as is presses against the load cell. Friction then prevents it from returning to its original position, which keeps a load on the load cell even after the test is completed. The friction would also prevent the the rig from measuring the correct value during the test itself.

The rig was not a complete failure, and the fact that it was correctly able to detect the presence of absence of torque shows that it worked in principle. On the other hand, the errors were far to large to make reliable measurements of the motor torque.

A.4 Other Design

The design shown shown in figure A.1 is already the second iteration of the rig. In the first design, had the one side of the motor mounted on soft rubber washers, and the other side on a load cell.

There were however two main problems with the design. The first problem is that even while the motor is not running, the load cell is being loaded by the weight of the load cell. Although this is not necessarily a major problem, the load cell must be able accurately measure the signal (about 0.1 kg) with a large offset due to the weight of the motor (about 2.5 kg). Clearly a load cell far larger than the the signal is needed, which may result in a minor reduction in accuracy.

The second and far more serious problem with the the design was that the the load under load the load cell deflects slightly. This deflection put the motor and pump out of alignment. A transverse shear force is therefore experienced by coupling between the motor and the pump, rather than being measured by the load cell as desired.

The second design using the cradle ensured that the alignment was always correct even if the load cell deflects under the motor torque.

A.5 Conclusion

The decision to make a torque measurement rig using a load cell was to eliminate the high costs of the in-line rotary torque sensors. In hind sight perhaps it was the wrong decision, however we did not predict so many problems with the *home-made* rig. While the rig does work, the errors due to friction overshadow the actual torque readings. Although the in-line rotary torque sensors are not cheap, you get what you pay for with torque errors of less than 1% of full scale.

Appendix B

Torque Estimate by Modelling the Motors

This appendix aims to find the torque at the output of the motor and input to the pump, by modelling the motors. The equivalent circuit method is used, and the meanings of each circuit element are discussed. By performing locked rotor and no load tests (with and without the gearbox) on the motors, one is able to find the circuit element parameters. Finally the friction and windage of the motor both with and without the gearbox can be determined as the power at the load in the no load tests.

B.1 The Motor Equivalent Circuit

There are various methods that can be used to measure the efficiency of three-phase electric motors. The equivalent circuit method will be used in this chapter [1, 19–21]. The equivalent circuit is given in figure B.1.

The equivalent circuit shown in figure B.1 is very similar to the transformer equivalent circuit. However where a transformer has an electrical load, the induction motor has a mechanical load which is described by the term $R_2' \frac{1-s}{s}$.

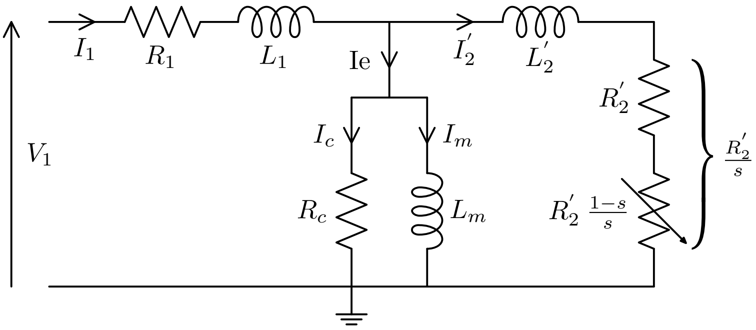

where

s = Rotor Slip
V_1 = Supply Voltage (V)
R_1 = Stator Resistance (Ω)
L_1 = Stator Leakage Inductance (H)
I_1 = Stator Current A
R_2' = Rotor Resistance (Ω)
L_2' = Rotor Leakage Inductance (H)
I_2' = Rotor Current (A)
R_c = Core Loss Branch (Ω)
I_c = Core Loss Current (A)
L_m = Magnetising Branch (H)
I_m = Magnetising Current (A)
I_e = Exciting Current (A)
Note: All rotor quantities have been referred to the stator.

Figure B.1: Three-phase induction motor per phase equivalent circuit

B.2 Meanings of the Circuit Elements

B.2.1 Copper Losses

The elements R_1 and R_2' (from figure B.1) represent the copper losses in the the motor. Whenever a current flows in a conductor there are resistive losses. These losses are present in both the stator and the rotor circuits.

B.2.2 Leakage Flux

The currents in both the rotor and stator circuits set up a flux. It is the interaction of these two fluxes that generates torque in the machine and causes rotation. Ideally one would like total coupling, however in reality this is not the case. The elements L_1 and $L_2^{'}$ (from figure B.1) represent the leakage flux in the motor. The leakage path is primarily in air, and therefore the leakage flux increases linearly with current [1].

These components do not directly cause any power loss, however they will reduce the power factor of the machine. This means that higher currents will be required to generate the same output power which would increase the copper losses.

B.2.3 Core Losses

The core loss component can be divided up into two sections, hysteresis and eddy current losses.

Hysteresis Losses

The hysteresis loss component is caused by the magnetic memory in the motors core. The energy lost per cycle is proportional to the volume of the material and the area of the associated hysteresis loop [1, 20, 21]. The power loss due to hysteresis is given in equation B.1.

$$P_h = Vol\ f \oint H\ dB \tag{B.1}$$

The area of the hysteresis loop is expressed empirically using a relationship from Charles P. Steinmetz [1, 20, 21] shown in equation B.2.

$$\oint H\ dB = \eta\ {B_m}^n \tag{B.2}$$

Finally B_m needs to be expressed in terms of V_c for the equivalent circuit. The relationship from equation B.3 holds true for sinusoidal excitation [1, 20, 21].

$$V_c = \sqrt{2}\, \pi\ f\ N\ A\ B_m \tag{B.3}$$

By combining equations B.1–B.3 we are able to determine the power loss due to hysteresis in the core. This is given by equation B.4.

$$\begin{aligned} P_h &= \eta\, Vol \left(\sqrt{2}\,\pi\, N\, A\right)^{-n} f^{1-n}\, {V_c}^n \\ &= k_h\, f^{1-n}\, {V_c}^n \end{aligned} \tag{B.4}$$

where

P_h = Hysteresis Loss in the Core (W)
Vol = Volume of the Core (m^3)
f = Supply Frequency (Hz)
H = Magnetic Field Intensity (A/m)
B = Peak Flux Density in the Core ($V.s/m^2$)
B_m = Peak Flux Density in the Core ($V.s/m^2$)
η = Hysteresis Coefficient of the Core Material
n = Hysteresis Exponent of the Core Material (1.5 – 2.5)
V_c = Voltage Across in the Core Windings (V)
N = Number of Turns in the Core Windings
A = Cross Sectional Area of the Core (m^2)
k_h = Lumped Hysteresis Coefficient

In most magnetic cores are constructed of heat-treated silicon steel, which has an inherently low hysteresis loss. After the heat-treated silicon steel is formed to the desired shape, the laminations are heated to a dull red and then allowed to cool. This process, known as annealing, reduces hysteresis losses to a very low value.

Eddy Current Losses

Eddy currents are currents induced in the core which oppose the changing magnetic field. The eddy current loss component is caused by the resistive losses in the core due to eddy currents [1, 20, 21]. The power loss due to eddy currents is given in equation B.5.

$$P_e = \frac{Vol\, \pi^2\, f^2\, T^2\, {B_m}^2}{6\,\rho} \tag{B.5}$$

Again B_m needs to be expressed in terms of V_c for the equivalent circuit. By combining equations B.5 and B.3 we are able to determine the power loss due to eddy currents in the core. This is given by equation B.6.

$$\begin{aligned} P_e &= \frac{Vol\, T^2\, {V_c}^2}{12\, \rho\, N^2\, A^2} \\ &= k_e\, {V_c}^2 \end{aligned} \tag{B.6}$$

where
P_e = Eddy Current Loss in the Core (W)
T = Lamination Thickness in the core(m)
ρ = Resistivity of the Core (Ω.m)
k_e = Lumped Eddy Current Coefficient (Ω^{-1})

In practice the eddy currents are minimised by using laminated cores since the eddy currents are reduced by decreasing the lamination thickness. The addition of a few percent (around 4%) of silicon to the core greatly increases the resistivity of the core steel, and also greatly reduces the eddy current losses [1].

Going back to the equivalent circuit in figure B.1, the core loss resistive element (R_c) must take both the hysteresis and eddy current losses into account.

$$R_c = \frac{1}{k_h\, f^{1-n}\, {V_c}^{n-2} + k_e} \tag{B.7}$$

B.2.4 Magnetizing Current

In an ideal transformer with no load on the secondary winding, there should be no current in the primary winding. However in reality a small magnetizing current is required to establish a magnetic flux. This is due to a finite reluctance of the magnetic core [1, 20, 21].

$$\Phi = \frac{N\, I}{\Re} \tag{B.8}$$

In an electric motor the same holds true The air gap between the stator and rotor however greatly increase the reluctance, and therefore the magnetising currents are significantly greater.

Note: Non-linearities in the core magnetic properties may cause harmonics in magnetising current and in the hysteresis loss component of the exciting current.

However these harmonics are usually relatively small, and have neglected in the model.

B.2.5 Mechanical Power

The mechanical power of the motor is represented by a variable resistor ($R_2 \frac{1-s}{s}$), which varies according to the mechanical load being driven by the motor. The rotor of an induction motor does not rotate at the same angular velocity as the stator magnetic field. The slip describes the difference between the rotor speed and the synchronous speed the stator flux. The slip is defined in equation B.9.

$$s = \frac{\omega_s - \omega}{\omega_s} \tag{B.9}$$

where

s = Normalised Motor Slip

ω = Actual Speed

ω_s = Synchronous Speed

If the rotor is running at synchronous speed, then the rotor will follow the stator flux. The rotor will therefore not experience a changing magnetic field, and no currents will be induced in the rotor. In the equivalent circuit, the variable resistor representing the mechanical load is open circuited at $s = 0$. This clearly models the case with no currents in the rotor.

On the other hand, if the rotor is locked it can essentially be regarded as a transformer with the secondary winding short circuited. Clearly no power can be transferred to a locked rotor, but the rotor currents will be high. In the equivalent circuit, the variable resistor representing the mechanical load is short circuited at $s = 1$.

During normal operation of the motor the slip will be a low value, since the rotor copper losses are directly proportional to the slip.

B.3 Finding the Equivalent Circuit Parameters

In order to complete the motor model for each of the two motors, the inductance and resistance values need to be determined. The stator resistance (R_1) can easily be measured using a multimeter. Both motors were operated with at rated current, for about five minutes, before the measurement was taken so that the measurement represents operating conditions of the motor [19]. The average resistance reading of the three-phases is used.

The remainder of the equivalent circuit parameters can usually be determined by performing a series of no load and locked rotor tests. Starting with the locked rotor test, the rotor currents ($I_2^{'}$) are significantly greater than the exciting currents (I_e). The exciting branch can therefore be neglected for simplicity at the cost of some accuracy. Also the it is difficult to separate the leakage fluxes (L_1 and $L_2^{'}$) without extensive testing so it is common to assume $L_1 = L_2^{'}$.

In the no load test is it common to assume that there are no rotor currents, and only the stator and core needs to be considered. Clearly this assumption is only valid at really low slip or if the motor is driven by another motor at synchronous speed. Also the magnetising current is significantly greater than the than the core loss current, so the core loss component is often neglected. The two simplified equivalent circuits are shown in figure B.2.

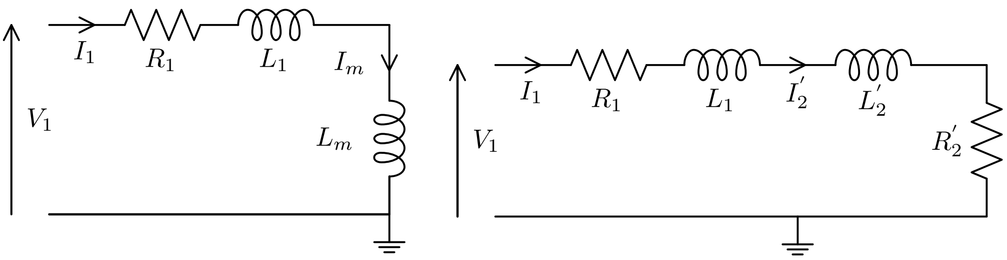

(a) The Simplified No Load Equivalent Circuit (b) The Simplified Locked Rotor Equivalent Circuit

Figure B.2: Simplified Equivalent Circuits

Without the aid of computers, it is difficult to try solve the circuit parameters any other way. However using Matlab many of the above simplifications are unnecessary and the complete circuit is evaluated for each test. Also since the motors being modelled are only 0.37 kW, the friction is relatively large and therefore the no load slip although small (about 0.005) should not be ignored.

For each motor a no load and locked rotor test was performed at 30, 40, 50 and 60 Hz. The results of the tests are given in table B.1.

Using both the genetic algorithm and simulated annealing algorithm from the Matlab Optimisation Toolbox the values of the equivalent circuit. Eight tests

Table B.1: Test Results used to Create the Motor Equivalent Circuit

Motor	Phase Voltage V	Phase Current A	Freq-uency Hz	Active Power W		Reactive Power VAr		Angular Velocity RPM	Gear Ratio	Slip %	Mechanical Power W
	52.63	0.9979	30.1	(132.42)	136.01	(75.52)	79.50	0.0	-	100	(0)
	59.17	1.0017	40.0	(143.70)	143.62	(105.50)	104.82	0.0	-	100	(0)
	64.17	0.9970	49.9	(143.19)	143.07	(129.14)	127.92	0.0	-	100	(0)
	71.02	1.0009	60.0	(147.38)	147.79	(158.42)	153.71	0.0	-	100	(0)
	149.68	1.0371	30.1	(124.31)	138.32	(378.31)	444.66	1788.1	1.00	0.9911	(26.39)
	193.75	0.9948	40.0	(137.96)	143.66	(489.82)	560.07	2381.8	1.00	0.7583	(34.81)
	240.25	1.0013	50.0	(157.60)	157.86	(610.76)	704.14	2980.4	1.00	0.6533	(46.79)
	279.99	0.8909	60.2	(168.85)	163.42	(694.92)	730.12	3591.2	1.00	0.5759	(56.53)
	148.57	0.9849	30.0	(151.86)	153.61	(364.42)	411.18	952.0	1.85	2.1556	(54.17)
	195.07	1.0001	40.0	(183.18)	181.53	(486.59)	556.37	1275.0	1.85	1.7188	(77.19)
	231.59	0.8462	50.0	(207.68)	189.32	(557.31)	556.50	1595.8	1.85	1.5923	(102.28)
	230.57	0.5882	60.0	(211.15)	221.33	(462.24)	316.29	1906.0	1.85	2.0528	(129.09)
	34.30	0.9386	30.1	(79.56)	79.59	(53.41)	54.70	0.0	-	100	(0)
	38.21	0.9377	39.9	(81.79)	81.18	(70.64)	70.46	0.0	-	100	(0)
	42.85	0.9390	50.0	(83.87)	83.78	(89.45)	86.89	0.0	-	100	(0)
	47.68	0.9418	60.0	(84.90)	86.14	(107.77)	103.54	0.0	-	100	(0)
	161.29	0.9463	30.3	(88.20)	88.32	(371.07)	449.26	1804.9	1.00	0.7206	(27.83)
	215.91	1.0107	40.0	(110.63)	115.26	(507.73)	644.39	2387.2	1.00	0.5333	(37.28)
	234.76	0.6486	50.0	(113.28)	101.98	(481.59)	445.23	2982.3	1.00	0.5900	(48.83)
	283.98	0.6695	60.0	(133.10)	127.96	(589.26)	555.75	3582.6	1.00	0.4833	(58.80)
	160.67	0.9382	30.1	(120.03)	140.97	(367.09)	429.65	961.0	1.85	1.5587	(58.48)
	212.70	0.9439	40.0	(153.15)	167.14	(489.34)	578.61	1281.6	1.85	1.2100	(80.68)
	230.58	0.6479	50.0	(168.57)	166.04	(462.04)	416.26	1600.0	1.85	1.3333	(104.43)
	230.01	0.5170	60.0	(186.21)	183.88	(385.02)	305.66	1912.3	1.85	1.7290	(133.55)

Note: The values enclosed by (..) are predicted by the equivalent circuit rather than measured values.

were performed for each motor, a locked rotor and a no load test at four different frequencies. These algorithms aim to tweak the equivalent circuit parameters in order to minimise the error between the equivalent circuit predictions and the actual measured values. Ideally we would like the model prediction and the actual measured values to be identical.

For a given equivalent circuit, are able to calculate both the active and reactive power, if we know the supply voltage, supply frequency and motor slip. The errors in the active and reactive power was chosen as the objective function (this also indirectly takes the error in the motor current into account). There errors for each of the eight tests is added. The objective function is given by equation B.10.

$$E = \sum_{i=1}^{8} \left(\left(\frac{P_{pred,i}}{P_{meas,i}} - 1 \right)^2 + \left(\frac{Q_{pred,i}}{Q_{meas,i}} - 1 \right)^2 \right) \tag{B.10}$$

where

E = Sum of Squares of Errors
P = Motor Active Power
Q = Motor Reactive Power
$pred$ = Parameter Predicted from the Equivalent Circuit
$meas$ = Parameter Measured During Testing

As stated above the values of R_1 were measured separately. Two assumptions were made $L_1 = L_2'$ and $n = 2$. The first assumption is standard practice, and without it the solver would tend to lump the inductances onto either L_1 or L_2' rather than appropriately dividing it. The second assumption the second assumption was made since it greatly reduces the complexity of the equation B.7, and hence the equivalent circuit. The value $n = 2$ is also the center value in the possible range of value for n [1, 20, 21]. Finally both assumptions reduce the number of parameters to be solved, greatly reducing the burden on the solver. The parameters of the equivalent circuit for each motor are given in table B.2.

The torque speed curves of the two motors are shown in figure B.5. Changing the frequency (and keeping V/f constant) will shift the torque speed curve left and right, while changing the voltage will scale the torque.

Table B.2: The Motor Equivalent Circuit Parameters

	Motor	
Parameter	**7070**	**9070**
R_1	31.20	14.80
$R_2^{'}$	19.41	17.64
L_1	0.0697	0.0523
$L_2^{'}$	0.0697	0.0523
L_m	0.795	1.023
k_h	0.0139	0.0144
k_e	0.0	0.0
n	2.0	2.0

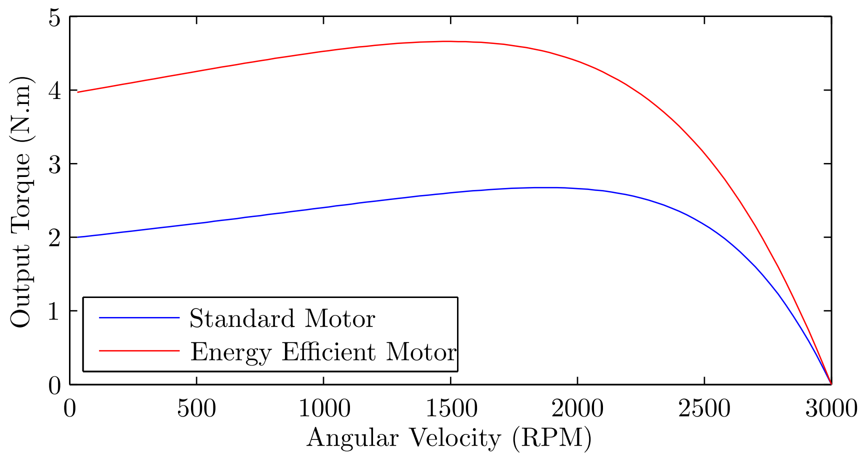

Figure B.3: Torque-Speed Curves at 230 V and 50 Hz

B.4 Friction and Windage

The model takes into account all losses in converting the power from electrical to mechanical. However part of the mechanical power will be lost to overcome the friction and windage, and only the remaining power will be available for the load. Figure B.4 shows the power flow in an induction motor [1].

The friction is usually proportional to the speed and the windage proportional to the square of the speed. Using the data from table B.1, the equivalent circuit is used to predict the mechanical power of the motor. Since all mechanical power is lost to overcome friction and windage (the tests were performed on no load), we are able to determine the friction and windage at four different speeds. By fitting a second order polynomial we can also predict the friction and windage losses at other speeds. Figure B.5 shows the friction and windage losses of each motor both with

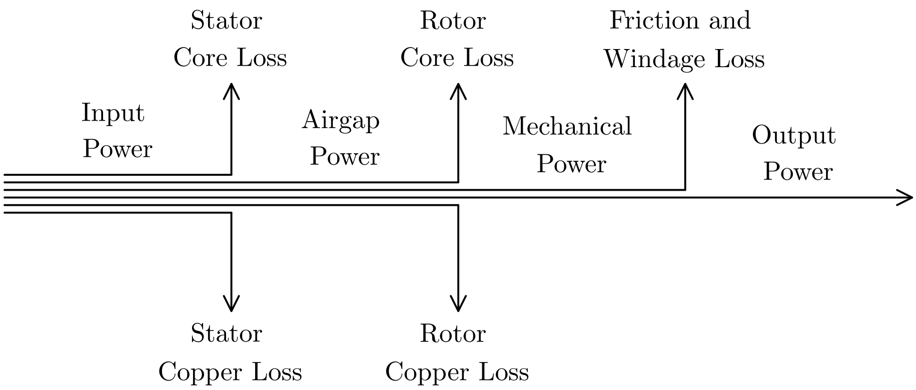

Figure B.4: Power Flow in an Induction Motor

and without the gearbox.

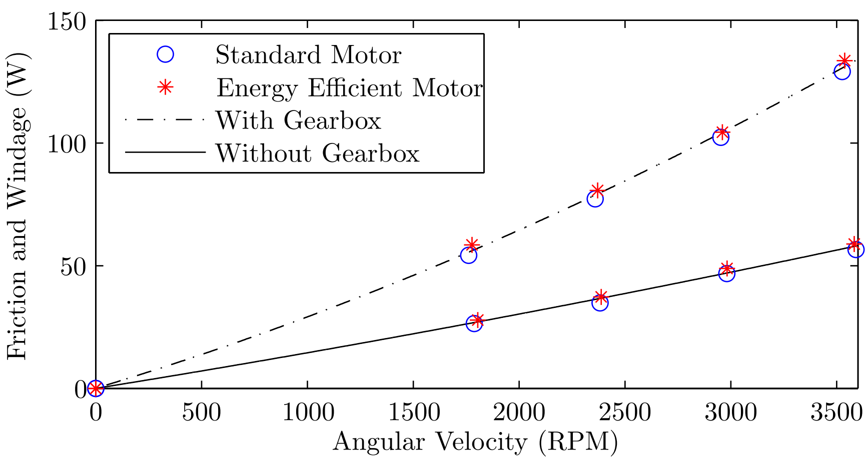

Figure B.5: Friction and Windage of each Motor, With and Without Gearbox

B.5 Conclusion

This appendix gave the procedure for modelling the standard and energy efficient motors using the equivalent circuit. A neural network solver was used to find the actual circuit elements of each motor. As expected the energy efficient motor has a higher torque and will therefore operate at a lower slip. Finally the friction and windage of the motor – in isolation and with coupled gearbox – was predicted at various operating speeds. A second order polynomial was then used to predict the friction and windage as a function of speed.

Appendix C

Torque Estimate by Modelling the Pump

The torque is estimated by modelling the pump in this appendix. Using the data sheet provided by the pump manufacturer, the input power and hence the torque can be found if one knows the pump flow rate and angular velocity. Since the data sheet only had curves at a few discrete angular velocities, the challenge was how to interpolate the values in between.

C.1 The Pump Curves

The torque can also be estimated by the pump characteristics. The curves given in figure C.1 were specified by the manufacturer. Only the bottom curve — which specifies the input power to the pump as a function of flow rate and angular velocity — is necessary.

Since the data sheet only specifies the relationship between flow rate and input power at a few distinct pump angular velocities it was necessary to find the missing values in between. Initially the approach was to use interpolation to find the missing values. Linear interpolation however did not seem like a good representation, especially since it was clear that the pump input power does not increase linearly with the pump RPM. And also between 900 and 2 000 RPM (the angular velocities at which the pump operates in the tests), the data sheet is very sparse, which only increases the problems with linear interpolation.

A polynomial seemed to be a better representation. Since no Matlab function exists

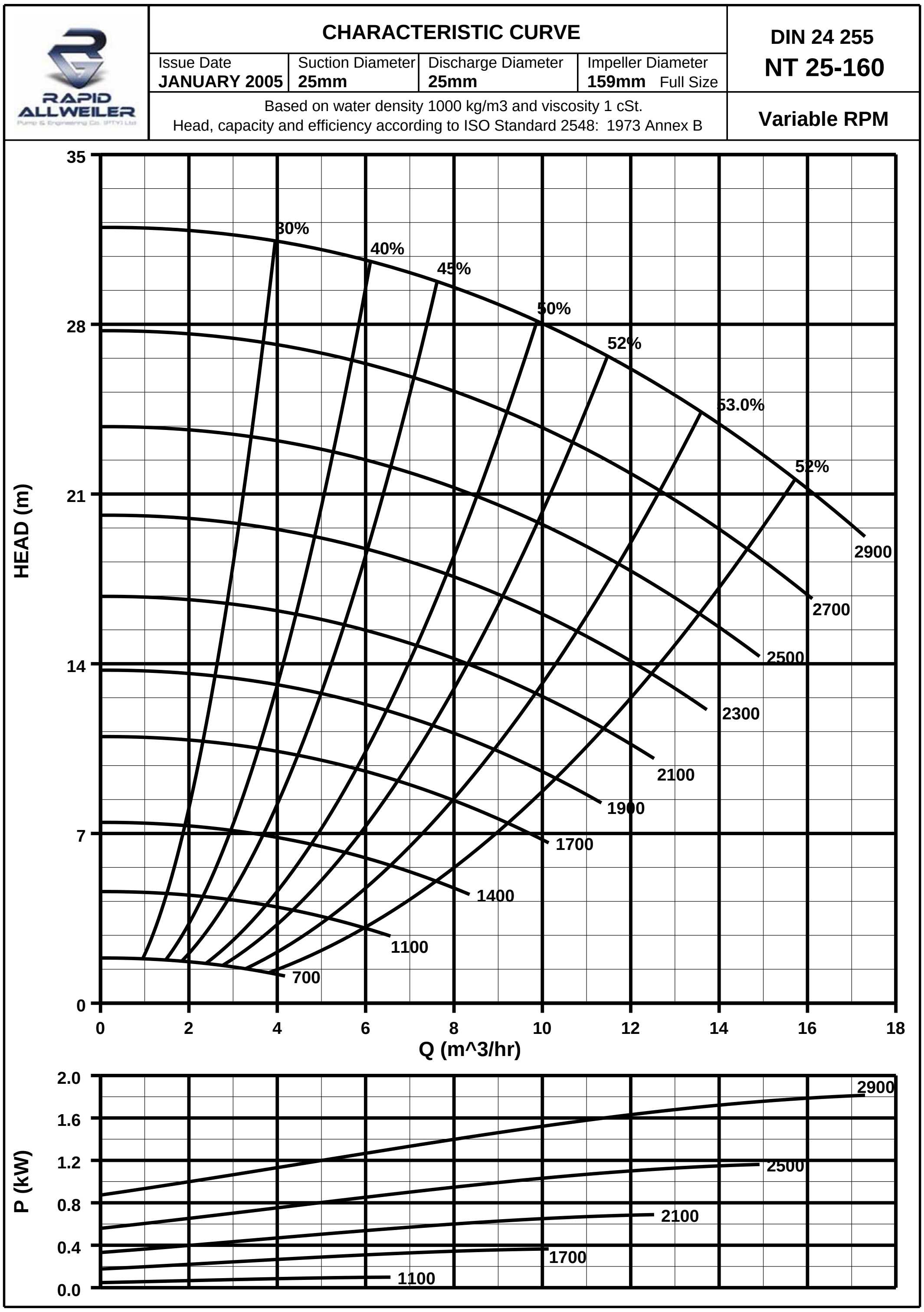

Figure C.1: The Rapid Allweiler Pump Data Sheet [15] which is which is able to fit a polynomial to a surface. Therefore a new function was written which bases on the existing *polyval* function. The polynomial is given in equation C.1.

$$
\begin{aligned}
P_{pump} = & -3.994{\times}10^{+0}\,Q^3\omega^4 + 2.670{\times}10^{-2}\,Q^2\omega^4 + 3.148{\times}10^{-5}\,Q^1\omega^4 \\
& + 6.926{\times}10^{-9}\,Q^0\omega^4 \\
& +2.492{\times}10^{+3}\,Q^3\omega^3 - 1.934{\times}10^{+1}\,Q^2\omega^3 + 2.278{\times}10^{-2}\,Q^1\omega^3 \\
& + 2.605{\times}10^{-5}\,Q^0\omega^3 \\
& -3.918{\times}10^{+5}\,Q^3\omega^2 + 4.552{\times}10^{+3}\,Q^2\omega^2 - 2.998{\times}10^{+0}\,Q^1\omega^2 \\
& + 1.218{\times}10^{-3}\,Q^0\omega^2 \\
& -1.570{\times}10^{+7}\,Q^3\omega^1 - 2.816{\times}10^{+5}\,Q^2\omega^1 + 4.092{\times}10^{+2}\,Q^1\omega^1 \\
& - 9.288{\times}10^{-2}\,Q^0\omega^1 \\
& +3.125{\times}10^{+5}\,Q^3\omega^0 - 9.690{\times}10^{+2}\,Q^2\omega^0 + 6.598{\times}10^{-1}\,Q^1\omega^0 \\
& - 2.662{\times}10^{-4}\,Q^0\omega^0
\end{aligned}
\tag{C.1}
$$

where

P_{pump} = Input Power to the Pump (W)

Q = Water Flow Pate (m^3/s)

ω = Pump Angular Velocity (rad/s)

The results of the polynomial in equation C.1 can be compared to the actual values from figure C.1. Figure C.2 is a visual representation of the polynomial and after dividing the power by the angular velocity we are able to determine the torque at the pump.

C.2 The Pump Curves

A 3–dimensional polynomial was found to get the intermediate values not given in the data sheet. This approach seems to provide a far better solution to using a linear interpolation approach, which does not take into account the curvature of the surface. It can be seen that the polynomial provides a really good fit to the values taken off the data sheet.

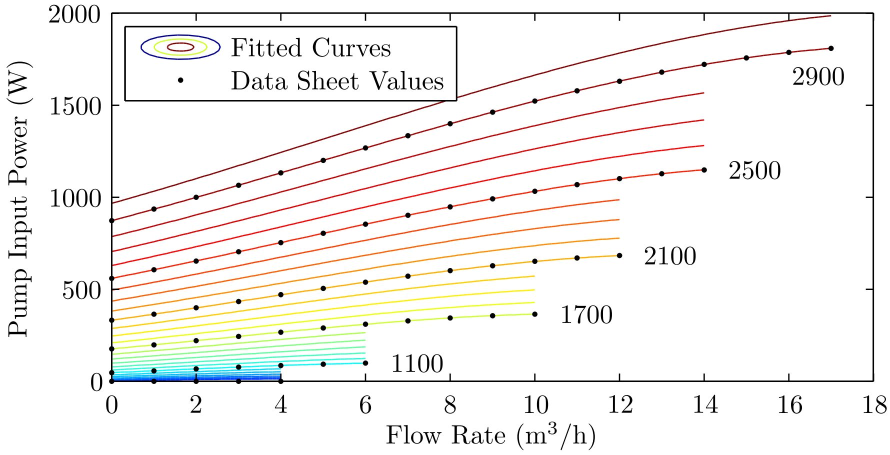

(a) The PDF

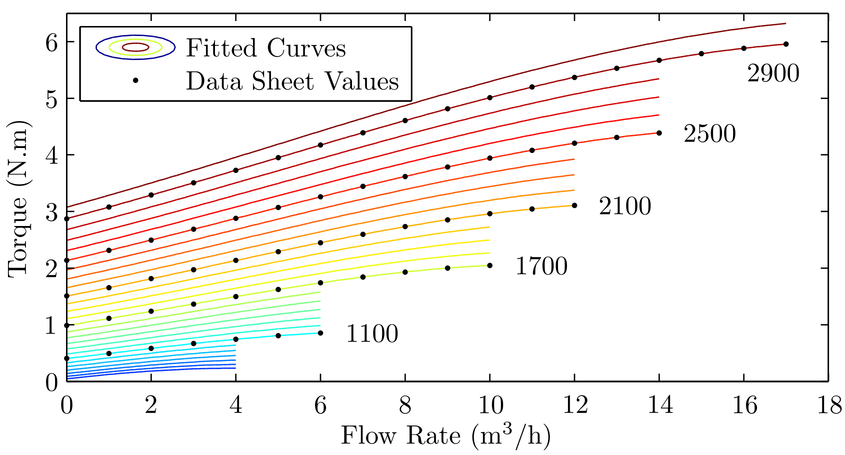

(b) The CDF

Figure C.2: An Example of the Uniform Distribution

Appendix D

Tabulated Pumping Test Results

The results of the pumping efficiency tests fit into a 96 by 28 table. The table has been split into six smaller tables – each a different subsystem – so that the table would fit into the document. The values in the table each represent the input conditions of each subsystem, for example the VSD voltage is the voltage at the input of the VSD, the output voltage of the VSD will be in the next table as the input voltage to the motor. There were some measurement errors for the final reading, so it has been left off the table.

The first column of each table is the key which can be used to align the rows of each separate table. The key is a unique four character code which indicates *(i)* the height that the water is pumped; *(ii)* the frequency at which the motor is operating; *(iii)* the position of the valve; and *(iv)* whether the standard or energy efficient motor was used.

- The first character indicates the height of the discharge tank. It is the number of flights of stairs that the discharge tank was raised to and ranges from 1 to 6.
- The second character indicates the frequency at which the VSD was operating. It ranges from 3 (for 30 Hz) to 6 (for 60 Hz) or X if the VSD has been bypassed.
- The third character indicates the position of the valve. O indicates that the valve is completely open, while V indicates that the ball valve is being used and has been set to about 45°.
- The fourth character indicates whether the standard or energy efficient motor was used for the test. S indicates that a standard motor was used, while E that an energy efficient motor was used.

Table D.1: Variable speed drive readings

	Variable Speed Drive				
Key	**Voltage** V	**Current** A	**Power** W	**Power Factor**	**Efficiency**
66OS	222.9	1.482	579.9	58.50%	98.68%
66OE	220.7	1.580	627.8	60.00%	98.71%
66VS	222.9	1.450	563.2	58.11%	98.50%
66VE	221.7	1.508	590.8	58.93%	98.64%
65OS	222.7	1.117	401.0	53.64%	97.49%
65OE	221.1	1.136	405.0	53.78%	97.30%
65VS	219.3	1.083	381.1	53.40%	97.29%
65VE	221.9	1.108	393.6	53.26%	97.25%
6XOS					
6XOE					
6XVS					
6XVE					
56OS	223.4	1.515	603.8	59.48%	98.73%
56OE	224.2	1.576	632.4	59.54%	98.66%
56VS	222.1	1.454	570.7	58.85%	98.63%
56VE	220.9	1.523	599.9	59.44%	98.59%
55OS	221.1	1.127	405.2	54.26%	97.32%
55OE	222.4	1.161	414.4	53.56%	97.34%
55VS	224.2	1.098	391.9	52.99%	97.24%
55VE	223.8	1.145	405.9	52.76%	97.36%
5XOS					
5XOE					
5XVS					
5XVE					
46OS	223.7	1.541	619.7	59.89%	98.72%
46OE	224.0	1.619	646.2	59.40%	98.65%
46VS	222.2	1.522	596.0	58.59%	98.66%
46VE	222.6	1.548	602.5	58.19%	98.66%
45OS	225.4	1.210	441.9	53.99%	97.52%
45OE	222.9	1.224	439.8	53.71%	97.32%
45VS	222.4	1.150	405.6	52.79%	97.30%
45VE	222.9	1.163	410.8	52.77%	97.38%
44OS	224.1	0.868	280.3	48.05%	94.61%
44OE	222.8	0.856	273.7	47.86%	94.80%
44VS	223.8	0.855	270.1	47.06%	94.72%
44VE	225.3	0.845	265.7	46.47%	94.49%

Key	Variable Speed Drive				
	Voltage V	Current A	Power W	Power Factor	Efficiency
4XOS					
4XOE					
4XVS					
4XVE					
36OS	221.9	1.669	680.9	61.30%	98.87%
36OE	221.1	1.631	659.2	60.89%	98.90%
36VS	222.4	1.529	603.5	59.12%	98.78%
36VE	221.5	1.559	616.9	59.53%	98.74%
35OS	223.0	1.225	454.1	55.34%	97.70%
35OE	221.7	1.222	446.4	54.88%	97.57%
35VS	222.1	1.135	411.2	54.37%	97.35%
35VE	222.4	1.166	419.0	53.86%	97.33%
34OS	223.7	0.885	296.9	50.06%	95.63%
34OE	221.5	0.881	284.9	48.61%	95.15%
34VS	223.0	0.839	276.8	49.23%	95.11%
34VE	222.6	0.843	273.1	48.46%	94.85%
3XOS					
3XOE					
3XVS					
3XVE					
26OS	223.7	1.601	640.1	59.55%	98.79%
26OE	223.2	1.623	658.0	60.48%	98.87%
26VS	224.8	1.557	618.2	58.80%	98.69%
26VE	220.5	1.584	635.2	60.59%	98.79%
25OS	223.5	1.200	438.7	54.47%	97.58%
25OE	224.8	1.228	449.8	54.29%	97.49%
25VS	223.3	1.172	423.4	53.90%	97.40%
25VE	222.3	1.208	435.2	54.01%	97.53%
24OS	224.0	0.887	294.8	49.47%	94.92%
24OE	221.4	0.894	287.9	48.43%	95.37%
24VS	222.5	0.875	286.4	48.96%	95.11%
24VE	222.8	0.885	279.7	47.28%	95.11%
23OS	222.4	0.664	187.9	42.41%	91.40%
23OE	220.7	0.638	179.0	42.36%	91.10%
23VS	222.5	0.633	186.7	44.20%	91.22%
23VE	222.5	0.651	176.7	40.66%	90.78%

Key	Variable Speed Drive				
	Voltage V	Current A	Power W	Power Factor	Efficiency
2XOS					
2XOE					
2XVS					
2XVE					
16OS	223.8	1.715	714.7	62.07%	98.93%
16OE	222.8	1.729	719.2	62.27%	98.88%
16VS	221.1	1.559	626.8	60.55%	98.67%
16VE	223.7	1.604	639.8	59.44%	98.44%
15OS	223.3	1.268	480.9	56.58%	97.90%
15OE	223.9	1.286	482.6	55.79%	97.80%
15VS	222.2	1.185	434.9	55.03%	97.29%
15VE	223.3	1.226	443.3	53.95%	97.47%
14OS	223.8	0.932	321.2	51.35%	95.64%
14OE	221.1	0.956	312.0	49.17%	95.92%
14VS	223.7	0.897	298.5	49.70%	95.25%
14VE	222.8	0.911	294.3	48.28%	95.28%
13OS	221.0	0.648	204.1	47.43%	91.75%
13OE	223.7	0.676	194.9	42.97%	91.87%
13VS	221.5	0.649	196.2	45.52%	91.71%
13VE	226.4	0.625	189.4	44.70%	90.70%
1XOS					
1XOE					
1XVS					
1XVE					

Table D.2: Motor readings

Key	Motor					
	Voltage V	Current A	Frequency Hz	Power W	Power Factor	Efficiency
66OS	242.8	1.021	60.00	572.3	77.00%	51.23%
66OE	238.5	1.121	60.00	619.7	77.31%	52.55%
66VS	242.5	0.993	60.00	554.8	76.79%	51.31%
66VE	240.7	1.049	60.00	582.8	76.97%	54.20%
65OS	246.9	0.835	50.00	391.0	63.20%	50.85%
65OE	243.1	0.816	50.00	394.1	66.23%	53.26%
65VS	242.2	0.798	50.00	370.8	63.96%	52.62%
65VE	245.0	0.801	50.00	382.8	64.99%	53.51%

Key	Motor					
	Voltage V	Current A	Frequency Hz	Power W	Power Factor	Efficiency
6XOS	231.9	0.909	50.00	402.7	63.68%	50.24%
6XOE	233.0	0.841	50.03	398.2	67.71%	53.95%
6XVS	232.7	0.908	49.96	391.0	61.70%	51.54%
6XVE	233.8	0.829	50.03	385.6	66.31%	54.41%
56OS	242.3	1.065	60.00	596.1	77.02%	49.72%
56OE	242.8	1.112	60.00	623.9	77.07%	54.10%
56VS	242.1	1.007	60.00	562.8	76.98%	51.40%
56VE	239.6	1.068	60.00	591.5	77.10%	53.96%
55OS	243.2	0.826	50.00	394.4	65.47%	52.29%
55OE	244.5	0.827	50.00	403.4	66.48%	54.37%
55VS	247.7	0.823	50.00	381.1	62.30%	53.06%
55VE	246.6	0.817	50.00	395.2	65.33%	53.38%
5XOS	230.6	0.908	50.00	409.9	65.27%	51.79%
5XOE	233.2	0.853	49.89	407.0	68.21%	54.51%
5XVS	233.3	0.917	50.03	400.7	62.42%	51.62%
5XVE	233.7	0.841	49.91	394.8	66.98%	53.99%
46OS	243.2	1.085	60.00	611.8	77.31%	49.82%
46OE	242.5	1.135	60.00	637.5	77.22%	53.80%
46VS	241.9	1.051	60.00	588.1	77.10%	49.76%
46VE	241.8	1.066	60.00	594.4	76.89%	54.54%
45OS	248.2	0.885	50.00	430.9	65.47%	49.91%
45OE	245.2	0.861	50.00	428.0	67.58%	52.82%
45VS	245.4	0.831	50.00	394.7	64.53%	52.48%
45VE	246.1	0.824	50.00	400.1	65.79%	53.82%
44OS	227.5	0.808	40.00	265.2	48.12%	44.16%
44OE	227.5	0.747	40.00	259.4	50.85%	47.12%
44VS	227.5	0.798	40.00	255.8	46.97%	45.14%
44VE	228.8	0.736	40.00	251.1	49.71%	47.50%
4XOS	233.6	0.952	49.91	434.8	65.20%	50.41%
4XOE	233.0	0.872	49.98	425.2	69.74%	54.00%
4XVS	234.0	0.942	49.90	417.1	63.06%	50.84%
4XVE	236.2	0.858	50.05	407.9	67.07%	54.03%
36OS	240.5	1.202	60.00	673.2	77.69%	44.51%
36OE	239.3	1.170	60.00	652.0	77.67%	52.83%
36VS	241.9	1.064	60.00	596.2	77.24%	49.39%
36VE	241.2	1.089	60.00	609.1	77.37%	54.09%

Key	Motor					
	Voltage V	**Current** A	**Frequency** Hz	**Power** W	**Power Factor**	**Efficiency**
35OS	245.6	0.895	50.00	443.7	67.29%	49.37%
35OE	243.6	0.870	50.00	435.5	68.51%	53.04%
35VS	244.8	0.840	50.00	400.3	64.94%	52.41%
35VE	245.8	0.834	50.00	407.9	66.28%	53.94%
34OS	227.9	0.840	40.00	284.0	49.44%	43.81%
34OE	226.6	0.761	40.00	271.1	52.44%	47.68%
34VS	226.9	0.810	40.00	263.2	47.76%	45.66%
34VE	228.2	0.752	40.00	259.0	50.30%	48.06%
3XOS	232.9	0.961	49.89	446.9	66.57%	50.15%
3XOE	232.0	0.881	49.98	434.8	70.88%	54.21%
3XVS	233.0	0.933	49.96	417.2	63.99%	51.46%
3XVE	233.9	0.854	49.99	407.4	67.96%	54.89%
26OS	243.2	1.120	60.00	632.4	77.45%	49.39%
26OE	241.6	1.159	60.00	650.5	77.47%	54.35%
26VS	244.5	1.078	60.00	610.1	77.19%	49.87%
26VE	238.5	1.133	60.00	627.6	77.45%	53.46%
250S	245.7	0.873	50.00	428.1	66.58%	52.39%
250E	246.9	0.874	50.00	438.5	67.78%	54.25%
25VS	245.8	0.855	50.00	412.4	65.39%	52.31%
25VE	243.9	0.856	50.00	424.4	67.82%	53.34%
240S	227.4	0.825	40.00	279.8	49.77%	46.34%
240E	226.1	0.764	40.00	274.6	53.03%	49.05%
24VS	226.5	0.819	40.00	272.3	48.93%	45.91%
24VE	227.3	0.756	40.00	266.0	51.62%	48.82%
230S	197.9	0.763	30.00	171.7	37.89%	36.77%
230E	197.9	0.698	30.00	163.1	39.37%	39.97%
23VS	198.0	0.766	30.00	170.3	37.44%	36.15%
23VE	198.6	0.693	30.00	160.4	38.81%	39.60%
2M0S	232.4	0.957	50.08	452.5	67.80%	51.15%
2M0E	230.2	0.884	49.88	436.9	71.59%	55.04%
2XVS	234.1	0.956	50.00	436.0	64.97%	50.85%
2XVE	232.9	0.873	50.03	426.3	69.88%	54.38%
16OS	242.7	1.251	60.00	707.0	77.71%	43.49%
16OE	241.5	1.259	60.00	711.1	78.04%	49.86%
16VS	239.8	1.112	60.00	618.5	77.35%	47.71%
16VE	242.7	1.123	60.00	629.8	77.17%	52.01%

Key	Motor					
	Voltage V	Current A	Frequency Hz	Power W	Power Factor	Efficiency
15OS	245.2	0.930	50.00	470.8	68.89%	48.18%
15OE	246.6	0.920	50.00	472.0	69.34%	51.21%
15VS	244.1	0.867	50.00	423.2	66.67%	50.75%
15VE	245.8	0.867	50.00	432.0	67.60%	51.01%
14OS	227.5	0.859	40.00	307.2	52.44%	43.17%
14OE	227.3	0.804	40.00	299.3	54.63%	46.34%
14VS	227.5	0.836	40.00	284.3	49.86%	44.20%
14VE	227.2	0.774	40.00	280.4	53.14%	45.43%
13OS	197.7	0.785	30.00	187.2	40.21%	35.53%
13OE	200.0	0.726	30.00	179.1	41.15%	38.68%
13VS	197.9	0.779	30.00	179.9	38.89%	35.40%
13VE	200.5	0.708	30.00	171.8	40.37%	37.37%
1XOS	231.9	0.976	49.98	471.3	69.45%	49.49%
1XOE	234.1	0.930	49.95	471.6	72.26%	52.07%
1XVS	234.5	0.973	50.07	453.9	66.34%	48.68%
1XVE						

Table D.3: Gearbox readings

Key	Gearbox		Combined
	Power W	Efficiency	Efficiency
66OS	293.2	78.10%	40.01%
66OE	325.7	79.30%	41.67%
66VS	284.7	77.33%	39.68%
66VE	315.8	78.44%	42.51%
65OS	198.8	72.80%	37.02%
65OE	209.9	73.64%	39.22%
65VS	195.1	72.29%	38.04%
65VE	204.8	72.93%	39.03%
6XOS	202.3	73.07%	36.71%
6XOE	214.8	73.99%	39.92%
6XVS	201.5	72.78%	37.51%
6XVE	209.8	73.27%	39.87%
56OS	296.4	78.54%	39.05%
56OE	337.5	79.94%	43.25%
56VS	289.3	77.72%	39.95%
56VE	319.2	78.72%	42.48%

Key	Gearbox		Combined
	Power W	Efficiency	Efficiency
55OS	206.2	73.96%	38.68%
55OE	219.3	74.82%	40.68%
55VS	202.2	73.24%	38.86%
55VE	210.9	73.74%	39.36%
5XOS	212.3	74.37%	38.52%
5XOE	221.9	74.98%	40.87%
5XVS	206.9	73.55%	37.97%
5XVE	213.2	73.88%	39.89%
46OS	304.8	79.09%	39.40%
46OE	342.9	80.30%	43.20%
46VS	292.6	78.17%	38.90%
46VE	324.2	79.05%	43.11%
45OS	215.1	74.99%	37.43%
45OE	226.1	75.62%	39.94%
45VS	207.1	74.02%	38.84%
45VE	215.3	74.32%	40.00%
44OS	117.1	65.33%	28.85%
44OE	122.3	66.16%	31.18%
44VS	115.5	64.79%	29.24%
44VE	119.3	65.26%	31.00%
4XOS	219.2	75.22%	37.92%
4XOE	229.6	75.83%	40.95%
4XVS	212.1	74.33%	37.79%
4XVE	220.4	74.62%	40.32%
36OS	299.7	79.15%	35.23%
36OE	344.4	80.54%	42.55%
36VS	294.5	78.27%	38.66%
36VE	329.5	79.37%	42.93%
35OS	219.0	75.61%	37.33%
35OE	231.0	76.23%	40.43%
35VS	209.8	74.33%	38.96%
35VE	220.0	74.86%	40.38%
34OS	124.4	67.47%	29.56%
34OE	129.2	68.08%	32.46%
34VS	120.2	66.20%	30.23%
34VE	124.5	66.73%	32.07%

Key	**Gearbox** Power W	**Gearbox** Efficiency	**Combined Efficiency**
3XOS	224.1	75.90%	38.06%
3XOE	235.7	76.47%	41.46%
3XVS	214.7	74.63%	38.40%
3XVE	223.6	75.07%	41.21%
26OS	312.3	79.78%	39.41%
26OE	353.6	80.98%	44.01%
26VS	304.3	78.94%	39.37%
26VE	335.5	79.92%	42.72%
250S	224.3	76.19%	39.91%
250E	237.9	76.89%	41.71%
25VS	215.7	75.11%	39.30%
25VE	226.4	75.69%	40.38%
240S	129.7	68.85%	31.91%
240E	134.7	69.40%	34.04%
24VS	125.0	67.60%	31.03%
24VE	129.9	68.19%	33.29%
230S	63.1	55.57%	20.43%
230E	65.2	56.27%	22.49%
23VS	61.6	54.38%	19.66%
23VE	63.5	55.06%	21.80%
2M0S	231.4	76.57%	39.17%
2M0E	240.5	77.01%	42.38%
2XVS	221.7	75.45%	38.36%
2XVE	231.8	75.97%	41.32%
16OS	307.5	79.80%	34.71%
16OE	354.6	81.16%	40.46%
16VS	295.1	78.55%	37.48%
16VE	327.6	79.27%	41.23%
15OS	226.8	76.60%	36.91%
15OE	241.7	77.30%	39.59%
15VS	214.8	75.05%	38.09%
15VE	220.4	74.98%	38.25%
14OS	132.6	69.72%	30.10%
14OE	138.7	70.34%	32.59%
14VS	125.7	67.84%	29.99%
14VE	127.4	67.63%	30.73%

Key	Gearbox Power W	Gearbox Efficiency	Combined Efficiency
13OS	66.5	58.11%	20.65%
13OE	69.3	58.96%	22.80%
13VS	63.7	56.06%	19.85%
13VE	64.2	55.70%	20.81%
1XOS	233.2	76.90%	38.06%
1XOE	245.6	77.49%	40.35%
1XVS	221.0	75.38%	36.69%
1XVE			

Note: The combined column is the efficiency of the both the motor and the gearbox combined.

Table D.4: Pump readings

Key	Pump Torque N.m	Pump angular Velocity rad/s	Pump Power W	Pump Efficiency
66OS	1.266	180.9	229.0	24.50%
66OE	1.379	187.3	258.2	25.73%
66VS	1.212	181.6	220.1	20.43%
66VE	1.313	188.7	247.7	19.91%
65OS	0.906	159.8	144.7	16.23%
65OE	0.951	162.5	154.6	17.81%
65VS	0.883	159.7	141.0	13.51%
65VE	0.918	162.7	149.4	13.70%
6XOS	0.920	160.6	147.8	16.74%
6XOE	0.971	163.6	159.0	18.47%
6XVS	0.908	161.5	146.7	14.17%
6XVE	0.937	164.0	153.7	14.12%
56OS	1.295	179.7	232.8	26.73%
56OE	1.436	187.9	269.8	27.98%
56VS	1.239	181.4	224.8	22.21%
56VE	1.334	188.3	251.3	21.02%
55OS	0.960	158.9	152.5	22.51%
55OE	1.011	162.2	164.1	23.53%
55VS	0.926	159.9	148.1	18.35%
55VE	0.957	162.6	155.5	18.15%

Key	**Pump** **Torque** N.m	**angular Velocity** rad/s	**Power** W	**Efficiency**
5XOS	0.984	160.5	157.9	23.00%
5XOE	1.022	162.8	166.4	23.80%
5XVS	0.944	161.1	152.1	18.72%
5XVE	0.965	163.2	157.5	18.35%
46OS	1.340	179.9	241.1	28.47%
46OE	1.468	187.6	275.4	29.10%
46VS	1.269	180.3	228.7	25.89%
46VE	1.361	188.3	256.3	23.43%
45OS	1.014	159.1	161.3	26.40%
45OE	1.055	162.0	170.9	26.76%
45VS	0.963	159.2	153.3	22.66%
45VE	0.986	162.4	160.0	21.27%
44OS	0.593	129.1	76.5	16.52%
44OE	0.618	130.9	80.9	17.78%
44VS	0.579	129.2	74.8	13.93%
44VE	0.594	131.0	77.8	13.58%
4XOS	1.029	160.3	164.8	26.32%
4XOE	1.069	162.8	174.1	27.06%
4XVS	0.982	160.5	157.6	22.88%
4XVE	1.004	163.8	164.5	21.41%
36OS	1.337	177.4	237.2	29.41%
36OE	1.487	186.5	277.4	29.80%
36VS	1.277	180.5	230.5	25.56%
36VE	1.388	188.4	261.5	24.08%
35OS	1.046	158.3	165.6	28.65%
35OE	1.090	161.6	176.1	28.73%
35VS	0.979	159.3	155.9	23.77%
35VE	1.014	162.4	164.7	23.64%
34OS	0.652	128.7	83.9	24.77%
34OE	0.674	130.6	88.0	24.97%
34VS	0.616	129.1	79.6	20.02%
34VE	0.634	131.0	83.1	19.90%
3XOS	1.065	159.6	170.1	28.77%
3XOE	1.108	162.7	180.2	28.80%
3XVS	0.998	160.6	160.2	24.03%
3XVE	1.028	163.4	167.9	23.74%

Key	Pump			
	Torque	angular Velocity	Power	Efficiency
	N.m	rad/s	W	
26OS	1.394	178.8	249.2	30.27%
26OE	1.531	187.0	286.3	30.41%
26VS	1.330	180.6	240.2	27.65%
26VE	1.432	187.2	268.1	27.67%
25OS	1.079	158.3	170.9	29.34%
25OE	1.131	161.7	182.9	29.99%
25VS	1.020	158.9	162.1	26.80%
25VE	1.059	161.8	171.4	27.09%
24OS	0.695	128.6	89.3	28.39%
24OE	0.716	130.5	93.5	28.13%
24VS	0.656	128.8	84.5	24.96%
24VE	0.677	130.8	88.6	25.29%
23OS	0.362	96.9	35.1	23.13%
23OE	0.374	98.1	36.7	23.50%
23VS	0.345	97.0	33.5	19.86%
23VE	0.356	98.2	35.0	20.29%
2XOS	1.107	160.1	177.2	29.75%
2XOE	1.140	162.4	185.2	29.92%
2XVS	1.042	160.5	167.2	27.00%
2XVE	1.079	163.3	176.1	27.17%
16OS	1.389	176.7	245.4	30.37%
16OE	1.546	186.1	287.7	30.49%
16VS	1.295	179.0	231.8	27.17%
16VE	1.379	188.3	259.7	23.36%
15OS	1.102	157.6	173.8	30.29%
15OE	1.157	161.5	186.8	29.93%
15VS	1.015	158.7	161.2	26.91%
15VE	1.020	162.1	165.2	24.38%
14OS	0.722	128.0	92.5	29.74%
14OE	0.748	130.3	97.5	29.36%
14VS	0.663	128.6	85.3	25.72%
14VE	0.660	130.6	86.1	23.75%
13OS	0.401	96.4	38.7	26.94%
13OE	0.417	97.9	40.8	28.24%
13VS	0.369	96.7	35.7	24.70%
13VE	0.365	97.9	35.8	22.39%

Key	Pump			
	Torque N.m	angular Velocity rad/s	Power W	Efficiency
1XOS	1.126	159.3	179.4	30.30%
1XOE	1.172	162.3	190.3	30.60%
1XVS	1.038	160.5	166.6	27.07%
1XVE				

Table D.5: Pipe and valve readings

Key	Pipe and Valve			
	Pressure $\times 10^3$ Pa	Flow Rate $\times 10^{-6}$ m^3/s	Power W	Efficiency
66OS	104.1	538.9	56.10	74.87%
66OE	110.3	602.1	66.45	70.67%
66VS	110.2	408.0	44.97	70.74%
66VE	114.1	432.4	49.33	68.35%
65OS	84.0	279.5	23.49	92.79%
65OE	86.3	319.1	27.53	90.40%
65VS	84.9	224.2	19.05	91.77%
65VE	87.9	232.7	20.47	88.65%
6XOS	84.7	291.9	24.75	92.00%
6XOE	87.3	336.1	29.36	89.28%
6XVS	86.3	240.9	20.78	90.39%
6XVE	89.1	243.6	21.70	87.53%
56OS	98.2	633.6	62.24	64.81%
56OE	107.5	702.5	75.49	59.27%
56VS	106.2	470.4	49.94	60.00%
56VE	108.9	484.9	52.80	58.46%
55OS	79.8	430.5	34.34	79.83%
55OE	82.7	466.7	38.61	76.97%
55VS	83.3	326.3	27.18	76.49%
55VE	86.2	327.4	28.22	73.90%
5XOS	81.1	447.7	36.31	78.53%
5XOE	83.4	474.8	39.60	76.38%
5XVS	84.7	336.1	28.48	75.13%
5XVE	86.9	332.5	28.90	73.30%
46OS	95.0	722.1	68.64	52.25%
46OE	103.1	777.5	80.14	48.11%
46VS	105.1	563.4	59.23	47.23%
46VE	111.2	539.7	60.04	44.62%

Key	Pipe and Valve			
	Pressure	Flow Rate	Power	Efficiency
	$\times 10^3$ Pa	$\times 10^{-6}$ m^3/s	W	
45OS	76.9	553.9	42.58	64.55%
45OE	79.4	575.7	45.75	62.51%
45VS	80.2	432.9	34.74	61.87%
45VE	84.6	402.5	34.04	58.74%
44OS	54.1	233.4	12.64	91.73%
44OE	55.4	259.3	14.38	89.57%
44VS	54.9	189.8	10.42	90.47%
44VE	56.5	187.1	10.57	87.90%
4XOS	77.5	560.0	43.38	64.11%
4XOE	80.5	585.4	47.11	61.67%
4XVS	81.5	442.2	36.07	60.91%
4XVE	85.9	409.9	35.21	57.83%
36OS	88.8	785.3	69.75	39.88%
36OE	98.0	843.6	82.67	36.22%
36VS	102.4	575.0	58.91	34.61%
36VE	106.2	592.9	62.99	33.39%
35OS	72.7	652.6	47.45	48.73%
35OE	75.6	669.0	50.60	46.92%
35VS	79.2	468.1	37.07	44.80%
35VE	82.9	469.5	38.94	42.81%
34OS	50.5	411.3	20.79	70.25%
34OE	51.9	423.2	21.97	68.35%
34VS	53.1	299.7	15.93	66.76%
34VE	54.8	301.6	16.53	64.77%
3XOS	73.8	663.1	48.94	48.04%
3XOE	76.6	677.9	51.92	46.35%
3XVS	80.8	476.6	38.50	43.94%
3XVE	83.9	474.9	39.86	42.29%
26OS	86.8	868.8	75.42	24.43%
26OE	94.7	919.3	87.07	22.35%
26VS	97.4	681.7	66.43	21.75%
26VE	104.0	713.6	74.19	20.36%
25OS	68.4	732.4	50.13	31.03%
25OE	72.2	760.0	54.85	29.33%
25VS	75.6	574.1	43.43	28.06%
25VE	78.8	589.4	46.44	26.94%

Key	Pipe and Valve			
	Pressure $\times 10^3$ Pa	Flow Rate $\times 10^{-6}$ m^3/s	Power W	Efficiency
24OS	47.2	536.9	25.35	44.93%
24OE	48.2	545.9	26.29	44.02%
24VS	50.3	419.2	21.09	42.18%
24VE	52.0	430.3	22.40	40.78%
23OS	28.3	286.1	8.12	74.82%
23OE	29.0	296.8	8.62	73.04%
23VS	29.2	227.2	6.65	72.51%
23VE	30.0	236.2	7.09	70.68%
2XOS	70.4	748.6	52.73	30.08%
2XOE	72.6	763.3	55.41	29.22%
2XVS	77.4	583.6	45.16	27.38%
2XVE	80.2	596.9	47.85	26.45%
1XOS	81.3	916.2	74.53	8.62%
1XOE	89.9	975.7	87.74	7.77%
1XVS	96.8	650.5	62.97	7.22%
1XVE	105.0	577.8	60.66	6.72%
16OS	65.2	807.4	52.64	10.69%
16OE	67.6	827.0	55.92	10.32%
15VS	76.1	569.9	43.37	9.21%
15VE	82.2	490.3	40.29	8.56%
14OS	43.4	632.8	27.50	16.15%
14OE	44.5	643.1	28.64	15.83%
14VS	49.3	445.1	21.93	14.30%
14VE	53.1	385.1	20.46	13.23%
13OS	24.1	431.5	10.41	29.11%
13OE	25.6	449.9	11.53	27.47%
13VS	28.0	314.8	8.82	25.12%
13VE	29.4	272.0	8.01	23.71%
1XOS	66.6	815.6	54.35	10.55%
1XOE	69.4	839.0	58.23	10.12%
1XVS	78.2	577.0	45.10	9.00%
1XVE				

Table D.6: System output readings

Key	Output				Overall
	Head	Volume	Time	Power	Efficiency
	m	$\times 10^{-3}$ m^3	s	W	
66OS	7.962	106.2	197	42.00	7.243%
66OE	7.966	107.2	178	46.96	7.480%
66VS	7.963	106.5	261	31.81	5.648%
66VE	7.964	106.8	247	33.72	5.708%
65OS	7.966	107.3	384	21.80	5.435%
65OE	7.967	107.5	337	24.88	6.144%
65VS	7.966	107.2	478	17.49	4.588%
65VE	7.967	107.5	462	18.15	4.611%
6XOS	7.967	107.7	369	22.77	5.653%
6XOE	7.966	107.2	319	26.21	6.583%
6XVS	7.966	107.4	446	18.78	4.804%
6XVE	7.966	107.4	441	19.00	4.927%
56OS	6.504	106.4	168	40.34	6.681%
56OE	6.505	106.8	152	44.74	7.075%
56VS	6.507	107.3	228	29.96	5.251%
56VE	6.503	106.2	219	30.87	5.145%
55OS	6.504	106.4	247	27.42	6.765%
55OE	6.504	106.4	228	29.72	7.171%
55VS	6.508	107.7	330	20.79	5.304%
55VE	6.507	107.4	328	20.86	5.139%
5XOS	6.505	106.6	238	28.51	6.955%
5XOE	6.507	107.3	226	30.24	7.431%
5XVS	6.506	106.9	318	21.40	5.341%
5XVE	6.507	107.4	323	21.18	5.366%
46OS	5.073	106.9	148	35.86	5.787%
46OE	5.066	105.0	135	38.56	5.967%
46VS	5.071	106.5	189	27.97	4.693%
46VE	5.071	106.3	197	26.79	4.446%
45OS	5.069	105.8	191	27.49	6.220%
45OE	5.073	107.1	186	28.60	6.503%
45VS	5.071	106.5	246	21.49	5.299%
45VE	5.073	107.1	266	19.99	4.867%
44OS	5.073	107.1	459	11.59	4.136%
44OE	5.075	107.6	415	12.88	4.708%
44VS	5.074	107.4	566	9.43	3.492%
44VE	5.075	107.6	575	9.30	3.498%

Key	Output				Overall
	Head	Volume	Time	Power	Efficiency
	m	$\times 10^{-3}$ m^3	s	W	
4XOS	5.073	107.0	191	27.81	6.397%
4XOE	5.070	106.0	181	29.05	6.832%
4XVS	5.075	107.5	243	21.97	5.267%
4XVE	5.073	107.0	261	20.36	4.991%
36OS	3.619	105.2	134	27.82	4.086%
36OE	3.625	107.1	127	29.94	4.542%
36VS	3.623	106.4	185	20.39	3.379%
36VE	3.624	106.7	180	21.03	3.409%
35OS	3.621	105.7	162	23.13	5.092%
35OE	3.625	107.0	160	23.74	5.319%
35VS	3.624	106.8	228	16.61	4.040%
35VE	3.627	107.5	229	16.67	3.978%
34OS	3.626	107.4	261	14.60	4.918%
34OE	3.624	106.7	252	15.02	5.271%
34VS	3.625	107.0	357	10.63	3.842%
34VE	3.626	107.4	356	10.71	3.920%
3XOS	3.622	106.1	160	23.51	5.261%
3XOE	3.625	107.1	158	24.06	5.534%
3XVS	3.626	107.2	225	16.92	4.055%
3XVE	3.626	107.3	226	16.86	4.138%
26OS	2.167	106.9	123	18.43	2.879%
26OE	2.163	105.7	115	19.46	2.958%
26VS	2.165	106.3	156	14.45	2.337%
26VE	2.162	105.6	148	15.10	2.378%
25OS	2.169	107.7	147	15.55	3.545%
25OE	2.162	105.6	139	16.09	3.577%
25VS	2.168	107.4	187	12.19	2.878%
25VE	2.168	107.3	182	12.51	2.874%
24OS	2.167	106.9	199	11.39	3.863%
24OE	2.165	106.5	195	11.57	4.020%
24VS	2.168	107.3	256	8.90	3.107%
24VE	2.168	107.2	249	9.13	3.265%
23OS	2.168	107.3	375	6.07	3.232%
23OE	2.167	107.1	361	6.30	3.517%
23VS	2.168	107.4	473	4.82	2.582%
23VE	2.169	107.5	455	5.01	2.838%

Key	**Output**				**Overall**
	Head	**Volume**	**Time**	**Power**	**Efficiency**
	m	$\times 10^{-3}$ m^3	s	W	
2XOS	2.165	106.3	142	15.86	3.505%
2XOS	2.167	106.9	140	16.19	3.705%
2XOS	2.164	106.2	182	12.36	2.836%
2XOS	2.167	106.9	179	12.66	2.970%
16OS	0.717	106.3	116	6.43	0.899%
16OE	0.714	105.4	108	6.82	0.948%
16VS	0.714	105.4	162	4.54	0.725%
16VE	0.721	107.5	186	4.08	0.637%
15OS	0.712	105.0	130	5.63	1.171%
15OE	0.712	105.0	127	5.77	1.195%
15VS	0.716	106.0	186	3.99	0.918%
15VE	0.719	106.9	218	3.45	0.778%
14OS	0.717	106.3	168	4.44	1.382%
14OE	0.720	107.4	167	4.54	1.453%
14VS	0.720	107.3	241	3.14	1.051%
14VE	0.718	106.7	277	2.71	0.920%
13OS	0.718	106.6	247	3.03	1.486%
13OE	0.719	107.1	238	3.17	1.625%
13VS	0.719	107.0	340	2.22	1.130%
13VE	0.713	105.3	387	1.90	1.002%
1XOS	0.718	106.8	131	5.74	1.217%
1XOE	0.718	106.6	127	5.89	1.250%
1XVS	0.718	106.8	185	4.06	0.894%
1XVE					

References

[1] P. C. Sen, *Principles of Electric Machines and Power Electronics.* John Wiley & Sons, Inc., second ed., 1997.

[2] "Electricity price hike in south africa." www.southafricaweb.co.za/article/electricity-price-hike-south-africa, Last Accessed 2 August 2010.

[3] Eskom, "Demand side management." www.eskomdsm.co.za Last Accessed 2 August 2010.

[4] Eskom Demand Side Management (DSM), "Energy efficient motors programme." www.eskomdsm.co.za/sites/default/files/u1/EEMPfactsheet.pdf, Last Accessed 2 August 2010.

[5] B. Crompton, "Motor efficiency labelling scheme," 2002. www.brookcrompton.com/pdf-files/2219e_efflabelling_v1.pdf, Last Accessed 2 August 2010.

[6] H. J. Holtzhausen, "Embodied energy and its impact on architectural decisions," in *Sustainable Development and Planning III Vol 1 and Vol 2*, 2007. www.uj.ac.za/EN/Faculties/fada/departments/architecture/conferences/Documents/Confernce%20Paper.doc, Last Accessed 2 August 2010.

[7] G. Milne and C. Reardon, "Your home technical manual – design for lifestyle and the future," tech. rep., Commonwealth of Australia, Fourth Edition, 2008. www.yourhome.gov.au/technical/pubs/fs52.pdf, Last Accessed 2 August 2010.

[8] Canadian Architect, "Measures of sustainability." www.canadianarchitect.com/asf/perspectives_sustainibility/measures_of_sustainablity/measures_of_sustainablity_embodied.htm, Last Accessed 2 August 2010.

[9] B. Lawson, *Building Materials, Energy and the Environment: Towards Ecological Sustainable Development.* RAIA, Canberra, Australia, 1996.

[10] G. Baird, Andrew, Alcorn, and P. Haslam, "The energy embodied in building materials – updated new zealand coefficients and their significance," *IPENZ Transactions*, vol. 24, pp. 46–54, 1997. www.ipenz.org.nz/ipenz/publications/transactions/Transactions97/civil/7baird.pdf, Last Accessed 2 August 2010.

[11] P. Oldfield, "Tall buildings in numbers – tall buildings and embodied energy," *CTBUH Journal*, vol. 3, pp. 50–51, 2009. www.ctbuh.org/LinkClick.aspx?fileticket=mtjd4j7fG1s=&tabid=1211&language=en-US, Last Accessed 2 August 2010.

[12] "Embodied energy coefficients – alphabetical." www.victoria.ac.nz/cbpr/documents/pdfs/ee-coefficients.pdf, Last Accessed 2 August 2010.

[13] G. M. Clarke and D. Cooke, *A Basic Course in Statistics.* Arnold Publishers, Inc., fourth ed., England, 1998.

[14] R. A. Serway and R. J. Beichner, *Physics for Scientists and Engineers with Modern Physics.* Saunders College Publishing, fifth ed., Philadelphia, USA, 2000.

[15] Rapid Allweiler, "Pump characteristic curve," tech. rep., Rapid Allweiler, January 2005. www.rapidallweiler.co.za/pump%20curves/din24255/25160V.pdf, Last Accessed 2 August 2010.

[16] Eskom, "Palmiet pumped storage scheme," October 2005. www.eskom.co.za/content/Palmiet%20FA%20Pg%2001-08.pdf, Last Accessed.

[17] S. Lee, *Effects of Input Power Factor Correction on Variable Speed Drive Systems.* PhD thesis, Virginia Polytechnic Institute and State University, 17 February 1999.

[18] L. R. Brown, *Plan B 2.0: Rescuing a Planet Under Stress and a Civilization in Trouble.* W.W. Norton & Co., 2006. http://www.earth-policy.org/index.php?/books/pb2/pb2_table_of_contents Last Accessed 2 August 2010.

[19] S. 60034–2–1:2008, "Rotating electrical machines — part 2–1: Standard methods for determining losses and efficiency from tests (excluding machines for traction vehicles)," 2008.

[20] L. W. Matsch and J. D. Morgan, *Electromagnetic and Electromechanical Machines.* John Wiley & Sons, Inc., third ed., 1986.

[21] A. E. Fitzgerald, J. Charles kingsley, and S. D. Umans, *Electric Machinery.* McGraw-Hill Companies, Inc., sixth ed., 2003.